A MICROFLUIDIC DEVICE FOR CONTINUOUS CAPTURE AND CONCENTRATION OF PATHOGENS FROM WATER

A Dissertation

by

ASHWIN KUMAR BALASUBRAMANIAN

Submitted to the Office of Graduate Studies of
Texas A&M University
in partial fulfillment of the requirements for the degree of

DOCTOR OF PHILOSOPHY

May 2007

Major Subject: Mechanical Engineering

A MICROFLUIDIC DEVICE FOR CONTINUOUS CAPTURE AND CONCENTRATION OF PATHOGENS FROM WATER

A Dissertation

by

ASHWIN KUMAR BALASUBRAMANIAN

Submitted to the Office of Graduate Studies of
Texas A&M University
in partial fulfillment of the requirements for the degree of

DOCTOR OF PHILOSOPHY

Approved by:

Chair of Committee,	Ali Beskok
Committee Members,	Suresh D. Pillai
	Debjyoti Banerjee
	Obdulia Ley
Head of Department,	Dennis O'Neal

May 2007

Major Subject: Mechanical Engineering

ABSTRACT

A Microfluidic Device for Continuous Capture and Concentration of Pathogens from Water. (May 2007)

Ashwin Kumar Balasubramanian, B.Tech, Indian Institute of Technology;

M.S., Texas A&M University

Chair of Advisory Committee: Dr. Ali Beskok

A microfluidic device, based on electrophoretic transport and electrostatic trapping of charged particles, has been developed for continuous capture and concentration of microorganisms from water. A generic design, utilizing mobility and zeta potential measurements of various microorganisms exposed to different environmental conditions and physiological states, was employed. Water and buffer samples at pH values ranging from 5.2–7.0 were seeded with bacteria (*E. coli, Salmonella,* and *Pseudomonas*) and viruses (*MS-2* and *Echovirus*). Negative control and capture experiments were performed simultaneously using two identical devices. Both culture based methods and real-time PCR analysis were utilized to characterize the capture efficiency as a function of time, flowrate, and applied electric field. Based on differences between the capture and negative control data, capture efficiencies of 90% to 99% are reported for *E. coli, Salmonella, Pseudomonas*, and *MS-2*, while the capture efficiency for *Echovirus* was around 75%. Overall, the device exhibits 16.67 fold sample volume reduction within an hour at 6 mL/hr. This results in a concentration factor of 15

at 90% capture efficiency. Direct quantification of capture on the anode of the prototype microfluidic device was also performed by particle tracking using fluorescent microscopy. Based on image processing, the capture data at different locations on the electrode surface is quantified as a function of the wall shear stress at these locations, which is calculated using CFD simulations. Finally, the Faradaic processes in the microchannel due to electrochemical reactions are studied to predict the amount of electrophoresis in the system.

Scaling of the device to sample 5 L/hr can be achieved by stacking 835 identical microchannels. Power and wetted volume for the prototype and scaled devices are presented. The device can thus function either as a filtration unit or as a sample concentrator to enable the application of real-time detection sensor technologies. The ability to continuously sample water without chemical additives facilitates the use of this device in drinking water distribution systems. This work constitutes the first step in our development of a continuous, microbial capture and concentration system from large volumes of potable water.

DEDICATION

This dissertation is dedicated in loving memory to my late father, S. Balasubramanian, who was a professor of physics, in Chennai, India. He could not realize his dream of earning a doctorate degree due to financial constraints and I am proud to say that I am living his dream for him. He always taught me to strive for excellence and dedication in everything I did in life, and those lessons stood me in great stead throughout the course of my graduate studies.

ACKNOWLEDGEMENTS

I would like to express my sincere gratitude and appreciation for my graduate research advisor, Dr. Ali Beskok, without whose guidance and support, my research and overall growth as a professional would not have been possible. I would also like to thank Dr. Suresh Pillai and Kamlesh A. Soni for providing guidance and help with the microbiology part of my research. I also appreciate the help of Brian Bachmeyer and Dr. William Lackowski of the Mechanical Engineering Department, for guidance with fabrication. Finally, I would like to thank my family and my lab colleagues for moral support throughout the course of my studies.

TABLE OF CONTENTS

Page

Page

LIST OF FIGURES

Page

Page

Page

LIST OF TABLES

Page

Page

Page

INTRODUCTION

Water quality is critical for human health and habitation in numerous applications including the municipal water distribution systems, beverage and food industries, and space exploration missions. One of the major challenges is to have reliable, efficient and cost effective procedures for water quality monitoring that can detect pathogens in water distribution and/or storage systems in a continuous manner.

In a variety of industrial applications, the source water is subject to treatment and disinfection prior to being used in water distribution lines. In the bottled water industry, certain chemicals are added to water before bottling to satisfy the applicable safety standards. However, bottled water is subject to less rigorous testing and purity standards than the city tap water in terms of its microbiological quality [1]. Similarly, municipal water supplies can also be subject to accidental microbial contamination. For space habitation, metabolic and hygienic wastes from laundry, showers, urinals, oral hygiene and humidity condensates (considered gray water) are usually reclaimed for potable use [2]. Reclaimed water is extremely vulnerable from a microbiological perspective. Closed loop water recycling systems provide ideal environments for formation of biofilms that can facilitate the growth and survival of human pathogens, as well as those organisms that can cause deterioration of the distribution lines.

This dissertation follows the style of *Journal of Micromechanics and Microengineering*.

Technologies for monitoring the physical, chemical and microbial environments of such systems are of critical importance. An effective method of detecting microbial contamination is essential to maintaining the quality in these systems. Significant research has been carried out on the development of specific, sensitive and high throughput technologies to detect pathogens in water. These include biosensors, microarray technologies, and PCR-based assays [3, 4]. One of the key limitations associated with currently available pathogen detection technologies is the small volumes sampled by these methods (10 – 50 μL volume). Efficient detection requires pathogen levels in the analyzed volume to be within the sensitivity threshold of the detection assay. Hence, large volumes with dilute pathogen levels need to be sufficiently concentrated down to smaller volumes, for current detection methods to have any practical value. This requires development of pathogen non-specific (generic) concentration methods for microorganisms.

Most of the existing pathogen concentration methods are based on filtration. Although these methods allow filtration of large volumes of water, there are numerous difficulties associated with their use. These include procedural complexity (time and cost), variable efficiency of virus recovery, and the need for optimization of the filtration methods for detecting viruses, bacteria and protozoan organisms from water [5]. Filtration techniques can be divided into membrane separation, ion exchange, adsorption, distillation, and evaporation systems [6]. Distillation, evaporation and ion exchange techniques are less commonly used, due to their cost, low efficiency, and requirement of

high amounts of chemicals and energy [7, 8]. In membrane separation systems, the physical and chemical characteristics of the membrane, such as the pore size, distribution and charge, dictates the degree of filtration. Maintaining significant hydrostatic pressure drop is critical to achieving high filtration efficiency in these systems. The smaller the pore size, the smaller is the size of particles that can pass through the membrane. Pressure drop through the filter increases with decreasing the pore size. The pressure drop ΔP across a porous medium is represented in terms of the pore size (D) and the number of pores (N_p) as [9]

$$\Delta P \propto \frac{\dot{Q}^2}{N_p^2 D^4}, \tag{1}$$

where $\dot{Q}$ is the flow rate. From equation (1), it can be deduced that an order of magnitude decrease in the pore size requires approximately two to three orders of magnitudes increase in the pressure drop to maintain the flow at a fixed flowrate. This is due to the filter geometry, where the number of pores (N_p) typically increases by decreasing the pore size. Pore size of the membranes used in filtration systems dictates whether it is microfiltration (1 -5 μm), ultrafiltration (0.01 - 1 μm) or nanofiltration (1 – 10 nm) and the power requirements to maintain substantial flow in such filtration systems increases with decreasing pore size [10].

Pathogen concentration technologies, based on membrane filters have been reported in the literature (Table 1).

Table 1: Review of membrane filtration based recovery methods for pathogens (All efficiencies are based on plating of inlet and outlet suspensions).

Buffer Type	Filtration Type	Recovery Efficiency (%)
Tap/Distilled water	Microfiltration [11]	90 - 99 - *MS-2* 73 - 99.99 - *E.coli* 50 – 99 - *Influenza*
Tap Water	Microfiltration + charged alumina fiber [12]	99.7 - *MS-2* 99.999 - *E. coli*
Tap Water	Ultrafiltration + Chemical dispersant [13]	71 - 86 - *MS-2* 70 - 74 - *E. coli* 12 - 71 - *E. faecalis* 62 - 75 - S*almonella*
Buffered Saline Water	Ultrafiltration [5]	70 - 84 - *E. coli* 36 – 72 - *Salmonella* 38 – 73 -*T-1* 45 - 62 - *PP7*
Dechlorinated tap water (pH altered)	Microfiltration + Chemical surfactants [14]	52.9 - 99.9 - *E.coli* 94 - 96 - S*almonella*
Phosphate buffer	Ultrafiltration with addition of blocking agents [15]	22 - 62 - *T1* 38 - 78 - *PP7* 4 - 44 - *Polio virus*

It can be seen from Table 1 that a generic membrane filtration method with the ability to simultaneously concentrate all pathogens from water with large recovery percentages is difficult to achieve. Recovery of viruses, which are considerably smaller than the bacteria, is inconsistent and has large variations [6]. Most of the filtration methods use chemical additives to enhance recovery percentages and require extensive preconditioning procedures that make the system very complex and expensive to operate. Also, the filtration method needs to be optimized for specific microorganisms to make it suitable for use in real-time field applications. It must be noted that most of the recovery efficiency percentages quoted in Table 1 are based on culture based methods, obtained by comparison of outlet and inlet samples. As a result, dead cells as well as viable but uncultivable cells that might result from the addition of chemicals are often overlooked.

Other commonly used pathogen concentration techniques are based on the surface charge of bacterial cells and viruses. Several researchers attempted to develop electrophoresis and dielectrophoresis based capture/concentration methods in microfluidic systems. Electrokinetic based concentration technologies, reported in the literature have been outlined in Table 2.

Table 2: Review of electrophoresis/dielectrophoresis based concentration methods for pathogens.

Pathogen and Buffer type	Electrokinetic Method	Capture Efficiency
Pseudomonas fluorescens in NaCl	Electrophoresis using gold electrodes [16]	~ 3 – 4 x 10^4 CFU/mm^2 in 15 mins (Microscopy)
E. coli, *Bacillus subtilis, B. cereus*, and *B. megaterium* in NaCl + KOH	Insulator based dielectrophoresis [17]	Qualitative (Microscopy)
Erwinia Herbicola in histidine buffer	Isoelectric focusing [18]	1.5 – 1.8 concentration factors (Optical density measurements)
Erwinia Herbicola in histidine buffer	Electrophoresis using gold electrodes [19]	Qualitative (Microscopy)
Live and dead *E. coli* cells from DI water	Insulator based dielectrophoresis [20]	3.0 concentration factor (Optical density measurements)
E. coli, *B. globigii* from phosphate buffer and river water	Ceramic beads with antibody coating [21]	10 – 70 % capture (Plating and optical density measurements)

It can be noted from Table 2 that previous electrophoresis based concentration systems have predominantly used a high capacity buffer solution in order to stabilize the pH in the system. These systems have limited field use since they cannot be directly employed in municipal water distribution lines. Capture efficiencies of these devices were often specific to the pathogen type and additionally, some of these systems required large electric fields and could not be used in flow based systems.

It is well known that various bacteria, viruses and protozoa have a net negative surface charge [22-24]. The negative surface charges on bacterial cell surfaces arise by virtue of ionized phosphoryl and carboxylate substituents on the outer cell envelope macromolecules, which are exposed to the extracellular environment [25]. Gram negative bacteria for example, have an outer layer of lipopolysaccharide (LPS) which forms a highly charged surface that is stabilized by cation binding [26]. There are, however, exceptions to these generalizations. For example, some strains of *Stenotrophomonas maltophila* can have a net positive charge [27]. Bacterial surface charges can be modulated by the presence of antibiotics, presence of metal ions and high pH [28-34].

In this study, we present a generic microfluidic device to capture pathogens from water by exploiting their surface charges. When subjected to an electric field, the pathogens experience electrophoretic motion towards the anode due to their negative surface charges. Cells in close proximity to the electrode surface experience electrostatic, van der Waals, and hydrophobic interactions. These interactions can be characterized using the DLVO theory [35, 36]. Based on this theory, particle adhesion is described primarily by two interaction forces including the Lifshitz-van der Waals interactions (generally attractive) and electrostatic interactions that result from overlapping electric double layers between the bacterial cell and the solid substratum surface (attractive for oppositely charged surfaces). The double layer interaction originates from the Coulomb interaction between charged molecules, and its strength and range is often strongly affected by the surface charge of the bacterial cells and the ionic strength of the

surrounding medium. The double layer interactions are related to the zeta potential of adhering surfaces, distance between the cell and surface, and the Debye length [37-39]. In this study, we are primarily interested in capturing and concentrating pathogens from water. Hence, the microfluidic device design is based on electrophoretic mobility and zeta potential measurements of microorganisms suspended in water using Capillary Electrophoresis (CE). These measurements account for variations in zeta potentials between physiologically similar cells and enable us to design a device non-specific to various microorganisms often encountered in water distribution systems. Therefore, transport of cells towards the electrode is achieved by electrophoresis, while the cell capture is a result of van der Waals and electrostatic interactions.

Electrophoretic transport depends on the charge of the particles, pH and ionic strength of the solution. In a microchannel, pH gradients can be created by employing large voltages (above electrolysis potential of water) to generate H^+ ions by electrochemical reactions. The diffusion of the H^+ ions establishes a concentration gradient in the microchannel, thereby altering the pH in different parts of the bulk solution [19]. In a solution with pH gradients, charged particles under an applied electric field will move towards a location where they experience zero net charge. This point is known as the isoelectric point (IEP) [39]. The IEP is a characteristic property of charged species, and at pH values above the IEP, the species has a net negative surface charge and at pH values below the IEP, the species has a net positive surface charge. Bacterial cells and viruses generally have an IEP ~ 2 – 4 [40]. Hence, we expect the bacterial cells and viruses to have an overall negative surface charge at the pH values of the waters

used in this study (5.2≤ pH ≤ 7). Therefore, electrophoretic transport of pathogens in water will be effective for most negatively charged species, allowing us to develop a generic device, unspecific to the pathogen type.

Microorganism capture due to cell-surface interactions, including van der Waals and electrostatic interactions are strongly influenced by the pH and ionic strength of the suspending media. These interactions depend not only on the surface charge of the bacterial cells, but also on the surface charge of the electrode itself. The electrode material has an IEP, just like the bacterial cells. For example, gold, which is commonly used as an electrode material in microfluidic systems, has an IEP of ~ 6.0 [41]. Hence, at more basic pH conditions [> pH.7.0], the electrode material will have an inherent negative surface charge. Therefore, even though an external positive charge is applied to the anode, the electrostatic interactions at higher pH values are less attractive when compared to lower pH values. This results in weaker bacterial adhesion to surfaces using media with higher pH values.

The ionic strength of the medium influences the electrostatic interactions between the cell and the surface as well. The ionic strength is inversely proportional to the thickness of the electric double layer (EDL) formed around the surface of the electrode and the cell [39]. Hence, at larger ionic strengths, the cells have to get much closer to the electrode surface, in order to have increased electrostatic attraction due to overlapping double layers, when compared to lower ionic strengths. Therefore, capture in the microfluidic device will be higher at lower ionic strengths, where the cell and the surface have thicker EDL around their surfaces.

Considering the above mentioned pH and ionic strength effects on cell-surface interactions, we performed our studies using reclaimed water from NASA's water regeneration system at the Houston Space Center, three leading brands of bottled water and phosphate buffer as the suspending media. The pH and ionic strength of the different water types used in this study are provided in Table 3.

Table 3: pH and ionic strength of suspending media used in study.

Parameter	NASA Reclaimed Water	Bottled Water-1	Bottled Water-2	Bottled Water-3	Phosphate Buffer
pH	5.24	5.3	5.6	6.5	5.5
Ionic strength (mM)	0.02	0.61	0.69	0.43	0.96

Results presented in this paper are applicable to all types of water with pH values ranging from 5.2–7.0, and ionic strength in the range of 0.01 mM – 1 mM. The current study was focused on three different bacterial genera (*E. coli, Salmonella,* and *Pseudomonas*) and two viruses (*MS-2* and *Echovirus*). These microorganisms are commonly encountered in terrestrial and recycled water distribution systems in America. Even though the tests conducted in this study utilized the above mentioned microorganisms, the microfluidic capture and concentration device is applicable to all types of bacterial cells and viruses found in water since it is based on a generic design.

DELINEATING THE ZETA POTENTIALS OF ENVIRONMENTALLY RELEVANT STATES OF SELECTED BACTERIA IN WATER

INTRODUCTION

Microorganisms are known to adversely impact man-made and natural ecosystems by forming biofilms, bio-fouling, and by the persistence of pathogenic populations in water resources and foods [42-46]. The presence of pathogenic microbial populations within distribution lines and recreational water sources are a constant concern for the drinking water industry and regulatory agencies. They cause public health concerns as well as influence the disinfection efficiency of commonly used disinfectants within distribution systems [47-49]. The initial attachment of bacterial cells to the substrate is obviously the primary step in the development of biofilms. A better understanding of the underlying factors responsible for the attachment of bacterial cells to surfaces can lead to the development of novel pipe coating materials, or changing the hydrodynamic conditions within vulnerable spots of the distribution systems, or the development of novel intervention and decontamination procedures. Studies have shown that the attachment of viruses to a substrate such as an aquifer sediment particle is controlled by the virus type, pH, ionic concentration, presence of multivalent cations, and organic matter. Similarly, bacterial attachment to surfaces is thought to be mediated by surface texture, electrostatic, and hydrophobic interactions [50-54]. When the bacterial cells are in close proximity to the solid surface (<100 nm

from surface), apart from the electrostatic interactions, various other specific interaction processes like van der Waals interactions and hydrophobic interactions play a vital role in determining the adhesion process. However, electrophoretic transport and electrostatic interactions can play a vital role in situations where it is necessary to bring the bacterial cells closer to a solid surface from the bulk flow region, so that other interactions and adhesion can occur.

It is well known that various bacteria, viruses and protozoa have a net negative surface charge [55-57]. The negative surface charges on bacterial cell surfaces arise by virtue of ionized phosphoryl and carboxylate substituents on the outer cell envelope macromolecules, which are exposed to the extracellular environment [58]. Bacterial surface charges can be modulated by the presence of antibiotics, presence of metal ions and high pH [59-65]. In this study, we are interested primarily in understanding the effects of electrostatic interactions on bacterial adhesion from water. Since bacterial biofilm formation in municipal water systems is important, the electrophoretic mobility and the zeta potential of environmentally relevant states of bacterial cells in such water samples are worthy of investigation. Additionally, understanding the range of variations of zeta potentials of different stress states of bacterial cells present in water distribution systems will help in designing a generic filtration and concentration system based on electrophoretic transport [39].

Laser-Doppler-based measurements such as light scattering measurements using Zeta-PALS etc. have been used in the past to measure zeta potentials of colloidal particles suspended in high ionic strength buffers [66]. Size measurements performed

using DICM show that the bacterial cells used in this study have sizes greater than one micron, and hence Capillary Electrophoresis (CE) was found to be more reliable for zeta potential measurements in terms of its repeatability for larger particles. To our knowledge, there is no published information about the zeta potential measurements of bacteria in water. CE has been used in the past to separate different bacterial cells and proteins based on their electrophoretic mobility [67, 68]. High ionic strength buffers are thought to be essential for efficient separation using the CE [67, 69]. However, given the need to determine the zeta potentials of bacteria cells in water samples, the use of high ionic strength buffers was untenable. Since municipal water generally has appreciable ionic concentrations, we hypothesized that water could be utilized in lieu of a high ionic strength buffer. Traditionally, buffers with ionic strengths typically at 5-10 mM or higher are employed with CE [70-71].

The ionic strength of the water used in this study was calculated from the individual salt contents presented in Table 5 using the method outlined by Wilson et al. [72] to be 10.5 mM. This is comparable to the buffers used with CE, and hence, we were able to measure the electrophoretic mobilities and zeta potentials of bacterial cells suspended in water.

Table 4: Chemical characteristics of the drinking water sample used in the electrophoretic mobility measurements.

Constituent	Concentration
Calcium (Ca)	2 ppm
Magnesium (Mg)	< 1 ppm
Sodium (Na)	214 ppm
Potassium (K)	3 ppm
Boron (B)	0.85 ppm
Carbonate (CO_3)	12 ppm
Bicarbonate (HCO_3)	440 ppm
Sulphate (SO_4)	15 ppm
Chloride (Cl)	79 ppm
Nitrate-N (NO_3-N)	< 0.01 ppm
Phosphorous (P)	0.42 ppm
Iron (Fe)	0.01 ppm
Zinc (Zn)	< 0.01 ppm
Copper (Cu)	0.01 ppm
Manganese (Mn)	< 0.01 ppm
Arsenic (As)	< 0.01 ppm
Barium (Ba)	< 0.01 ppm
Nickel (Ni)	< 0.01 ppm
Cadmium (Cd)	< 0.01 ppm
Lead (Pb)	< 0.01 ppm
Chromium (Cr)	< 0.01 ppm
Fluoride (F)	0.58 ppm
Total Dissolved Salts	768 ppm
pH	8.40
Conductivity	838 μS/cm

Previous studies demonstrating the use of capillary electrophoresis to elucidate bacterial zeta potentials utilized laboratory prepared buffer solutions, and for the most part, these studies have used bacterial cells grown in typical “rich” laboratory media.

The present study is unique in that it has employed different bacterial genera grown or exposed to different nutrient conditions to simulate different environmental states of bacterial cells and their zeta potential was determined in realistic drinking water environments.

BACTERIAL STRAINS AND MEDIA

The following bacterial strains were employed in this study: *Escherichia coli* DH5α, *E. coli* DH5α labeled with GFP, *Salmonella* Newport, and *Pseudomonas aeruginosa* (ATCC 10145). The *E. coli* strains were obtained from our laboratory collection. *Salmonella* Newport was previously isolated in the environment in one of our previous studies [73]. *Pseudomonas aeruginosa* cells were obtained from ATCC culture collections. Unamended Luria-Bertani broth (LB) was used to grow *E. coli*, and *Salmonella* Newport, while LB amended with ampicillin (100 *μg/mL*) was used to grow GFP-labeled *E. coli* cells (Ampicillin was used to maintain the GFP plasmid). Tryptic Soy broth (TSB) was used to grow *Pseudomonas aeruginosa*.

Drinking Water Sample

City of College Station, Texas, water samples collected from a laboratory faucet on the Texas A&M University campus were used in the experiments. Five liters of tap water was collected at a time, filtered (0.2 μm) and stored refrigerated until use. Portions of these samples were also analyzed (prior to filtration) for standard water quality parameters such as pH, conductivity, total dissolved salts and charge balance at the Texas A&M University Soil, Water and Forage Testing Laboratory. The results of this analysis are presented in Table 5.

Preparation of Environmentally Relevant States of Bacterial Cells

Rich medium cells: Cells were grown overnight (100 ml of broth) at 37ºC (*E. coli*, *Pseudomonas aeruginosa*, *Salmonella* Newport) in a shaking water bath (100 rpm) in LB or TSB broth. The cells were pelleted by centrifugation (10 min, 6000×*g*) at room temperature. For washing, pelleted cells were resuspended in 25 ml of filtered tap water and centrifuged (10 min, 6000×*g*) at room temperature. The supernatant was decanted and the steps were repeated two more times. After washing, the cells were resuspended in 1 ml of sterile drinking water, and stored at 4 ºC and used in CE experiments within 48 hours. The supernatant obtained at the initial centrifugation step was filter sterilized using 0.22-µm filters and stored at 4 ºC. (The filter sterilized cell free supernatant was used as a negative control to verify that the electropherogram peaks during the mobility measurements were not arising from media components).

Minimal medium cells: To obtain cells exposed to nutrient limited conditions, the cells were grown overnight in minimal media at 37 ºC or 30 ºC in shaking water bath (100 rpm). The minimal medium was prepared as follows: 1 g of dextrose, 7.0 g of di-potassium phosphate, 2.0 g of mono-potassium phosphate, 0.5 g of sodium citrate, 0.1 g of magnesium sulphate, and 1.0 g of ammonium sulphate were dissolved in 1000 mL of deionized water and autoclaved. Following the initial incubation, the subsequent steps were similar to that used for the preparation of nutrient rich cells.

Starved cells: The cells were initially prepared similar to that of the "nutrient rich" conditions. The cells were then stored for 10 days at 4 °C in drinking water prior to the CE experiments.

Dead Cells: The cells were initially prepared similar to that of the "nutrient rich conditions". The cells were then "killed" using either sodium azide (1%) or exposing the cells to ionizing radiation (3.5 kGy) using electron beam source at Texas A&M University. We employed this method of killing since it is less destructive on the cell surface. The cells were defined as being "dead" or "non-viable" based on their inability to grow on LB or TS agar plates after 24 hour incubation at 37 °C.

MOBILITY AND ZETA POTENTIAL MEASUREMENTS

Electrophoresis is the motion of charged particles in ionic solutions under electric fields. Electrophoretic velocity is proportional to the electric field, and the proportionality constant is known as the electrophoretic mobility (μ_{EP}). Under high ionic strength, the mobility is given as

$$\mu_{EP} = \frac{q}{6\pi\eta R}, \tag{2}$$

where q is the surface charge, R is the cell radius, and η is the absolute viscosity of the suspending medium. Upon application of electric field, the bacterial cells in the capillary experience electrophoretic motion towards the anode due to their negative surface charges, and they also experience motion towards the cathode due to electroosmotic flow of the ionized liquid, created by the negative charges on the fused silica capillary walls. To distinguish between the electroosmotic and electrophoretic transport, electroosmotic

flow is measured by adding electrically neutral species to the sample. Dimethylsulphoxide (DMSO) was used as the electroosmotic flow marker in our experiments. The total or apparent mobility of a charged species is then expressed as the sum of the electrophoretic mobility and electroosmotic mobility, and is represented as

$$\mu_{APP} = \mu_{EP} + \mu_{EO} \ . \tag{3}$$

Migration time of the bacterial cells undergoing both electrophoretic and electroosmotic motion is represented as t (i.e. time required for the species to migrate from the injection end to the detector). The migration time of DMSO is dictated by the electroosmotic motion and it is represented as t_{EO}. The apparent mobility and electroosmotic mobility are then represented as

$$\mu_{APP} = \frac{L_d / t}{V / L_t}, \tag{4}$$

$$\mu_{EO} = \frac{L_d / t_{EO}}{V / L_t}, \tag{5}$$

where L_d is the length of the capillary column from injection to the detector, and L_t is the total length of the column from end to end. V is the applied voltage between the two electrodes. For the experiments performed, L_t = 56.68 cm and L_d = 50.08 cm were used. CE measures t and t_{EO} and equations (4) and (5) are used to calculate the apparent and electroosmotic mobility respectively. The electrophoretic mobility of the bacterial cells was then calculated as the difference between apparent and electroosmotic mobilities. A typical electropherogram obtained from a representative CE experiment is shown in

Figure 1 with the abscissa and ordinate representing the time in minutes and the absorbance at the UV detector in milliabsorbance units, respectively.

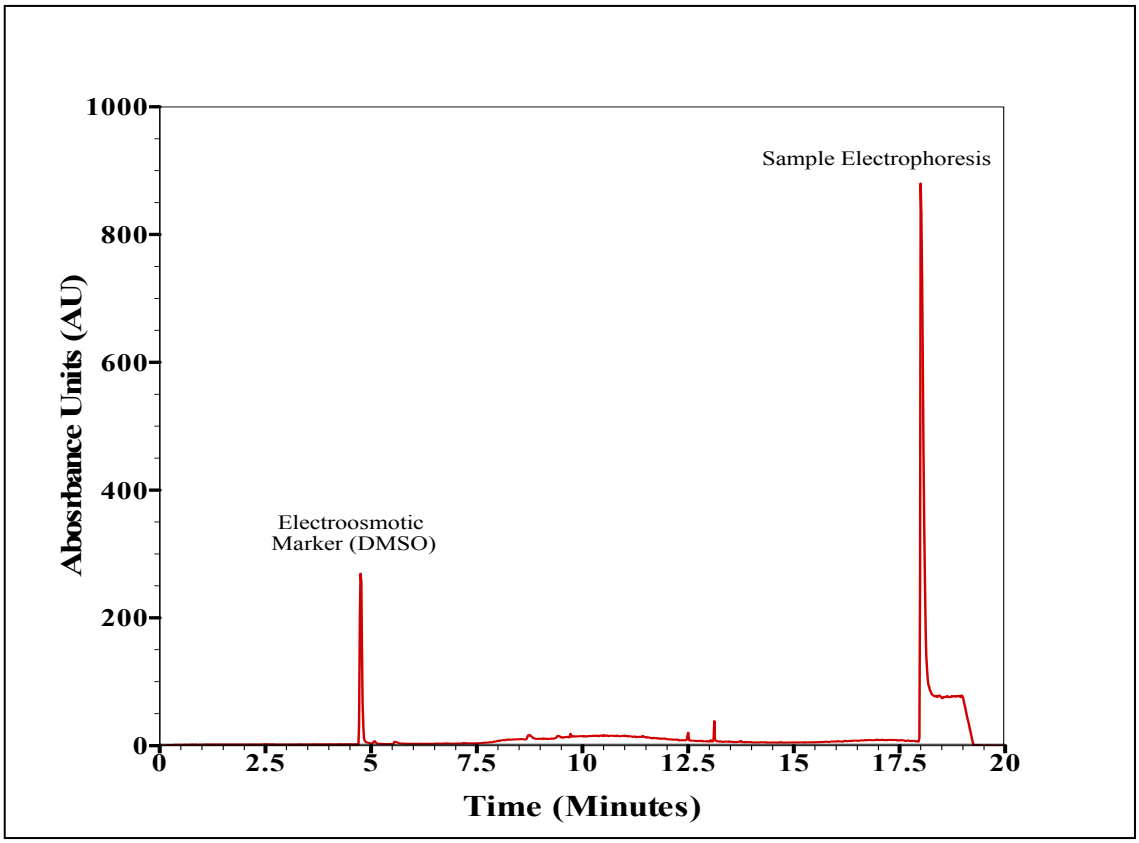

Figure 1: CE electropherogram plot of *E.coli* in rich medium (10^7 cfu/ml) with Dimethylsulphoxide (DMSO) added as an electroosmotic flow marker.

The zeta potential of the bacterial cells (ζ) is calculated using the electrophoretic mobility values as

$$\zeta = \frac{\mu_{EP}\eta}{\varepsilon}, \tag{6}$$

where μ_{EP} is the electrophoretic mobility calculated from equation (2), and ε is the dielectric permittivity of the drinking water.

CE Protocol

A Beckman P/ACE 5510 capillary zone electrophoresis unit, controlled by Beckman System software (Beckman P/ACE Station), was used to measure the electrophoretic mobility of different bacterial cell preparations. A standard calibration of the CE equipment was performed initially with standard test samples provided by the manufacturer. To this end, electrophoretic mobility measurements of 1 mg/ml of Bovine serum albumin (BSA) and 1 mg/ml of Insulin dissolved in 0.1 % TFA was performed.

The voltage needed for separation was determined prior to the actual experiments. Based on the Ohms law calibration using the drinking water sample (Figure 2), joules heating effects were observed beyond 22.5 kV. All of our separation experiments were carried out using a voltage of 20 kV.

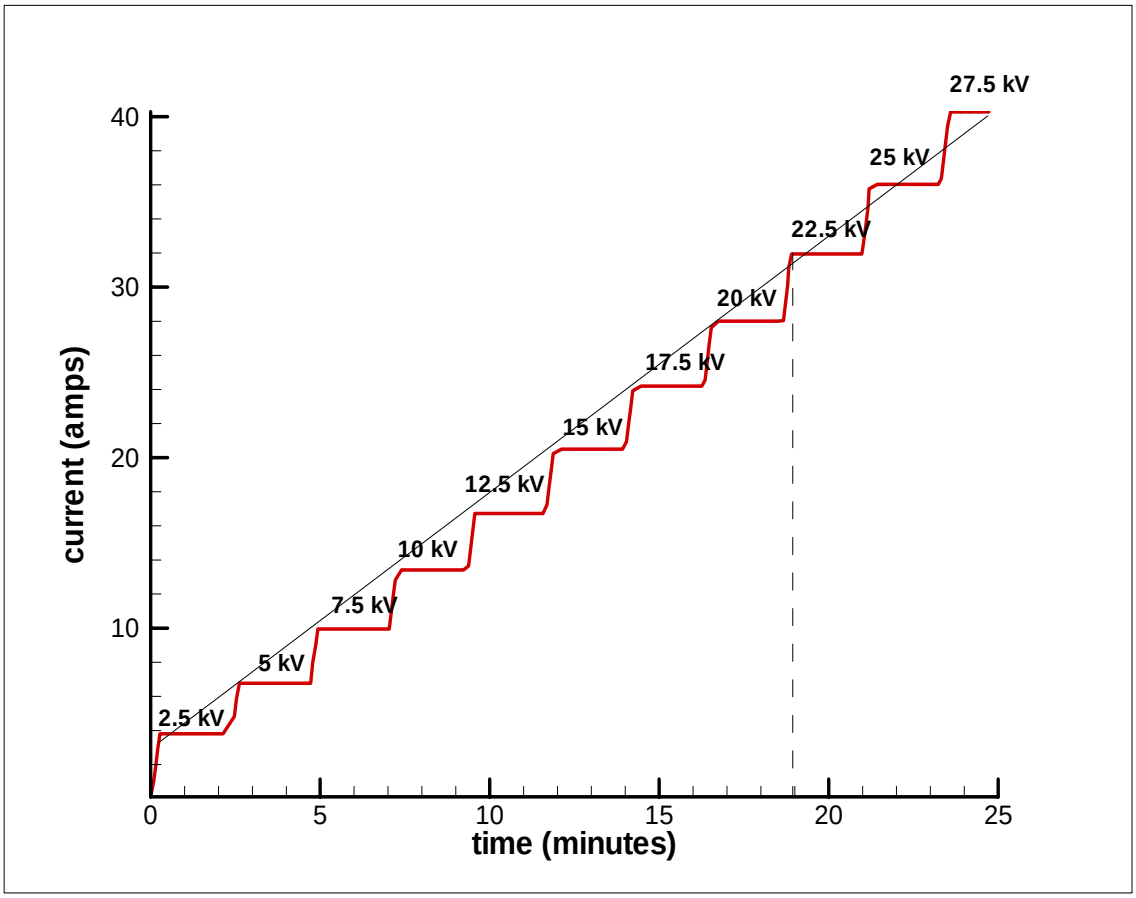

Figure 2: Ohms Law calibration with drinking water to determine voltage of separation with CE.

The samples were pressure injected into fused silica capillaries with an outer diameter of 300 μm and an inner diameter of 75 μm. DMSO (Dimethylsulphoxide) was first pressure injected into the capillary for a total of 3 seconds, followed by the sample

to be analyzed for 3 seconds. The DMSO is electrically neutral and is representative of the electroosmotic flow in the capillary. Prior to running a separation method each time, the capillary was rinsed with 1 M NaOH for 5 minutes, followed by a rinse with 0.1 M NaOH for 10 minutes, 10 minute rinse with deionized water, and finally, a 10 minute rinse with drinking water. At the end of each separation, 2 minutes rinse of the capillary with 0.1 M NaOH and deionized water were also performed. The separation itself was carried out for a total of 20 minutes using a voltage of 20 kV. Each bacterial cell preparation was analyzed in the CE three times to obtain a representation of the mean and standard deviation in the electrophoretic mobility values.

Results of Mobility Measurements

Based on preliminary experiments with the CE system, the detection sensitivity of the instrument was established as 10^6 CFU/ml. Also, the cell concentration did not have significant effects on the electrophoretic mobility. Higher concentration produced larger and wider peaks in the electropherograms (data not included). Tables 5 and 6 present the electrophoretic mobilities and the zeta potentials of different bacterial cells employed in this study, respectively.

Table 5: Electrophoretic mobility of different bacterial cells under various environmental states and growth conditions. Values represent mean ± standard error (*n* = *3*, ND= not done).

Bacteria	Medium			
	Rich (μm-cm/V-sec)	**Minimal (μm-cm/V-sec)**	**Starved (μm-cm/V-sec)**	**Dead (μm-cm/V-sec)**
E. coli	-3.8 ± 0.06	-3.13 ± 0.02	-3.19 ± 0.03	-3.37 ± 0.03
E. coli + GFP	-3.67 ± 0.06	ND	-3.47 ± 0.02	-3.6 ± 0.09
Salmonella sp.	-1.23 ± 0.12	-0.31 ± 0.03	-1.26 ± 0.19	-1.25 ± 0.19
Pseudomonas sp.	-3.72 ± 0.04	-3.74 ± 0.24	-3.17 ± 0.14	-3.3 ± 0.02

Table 6: Zeta potentials of different bacterial cells under various environmental states and growth conditions. Values represent mean ± standard error (*n* = *3*).

Bacteria	Medium			
	Rich (mV)	**Minimal (mV)**	**Starved (mV)**	**Dead (mV)**
E. coli	-3.8 ± 0.06	-3.13 ± 0.02	-3.19 ± 0.03	-3.37 ± 0.03
E. coli + GFP	-3.67 ± 0.06	ND	-3.47 ± 0.02	-3.6 ± 0.09
Salmonella sp.	-1.23 ± 0.12	-0.31 ± 0.03	-1.26 ± 0.19	-1.25 ± 0.19
Pseudomonas sp.	-3.72 ± 0.04	-3.74 ± 0.24	-3.17 ± 0.14	-3.3 ± 0.02

Salmonella sp. cells showed the lowest zeta potential compared to the other cells across the different physiological conditions. There was a significant difference in the zeta potential of *Salmonella* as compared to *E. coli* and *Pseudomonas* sp. when they were dead or exposed to rich, minimal or starved conditions. *E. coli and Pseudomonas* cells exposed to starved and minimal conditions show significant differences in their zeta potential values. It is interesting that the dead cells of the *E. coli* and *Pseudomonas* exhibited significant differences in their zeta potentials compared to the other growth conditions. *E. coli* cells, when labeled with GFP showed a significant increase in their zeta potential value in the starved medium, when compared to the unlabeled *E. coli* cells. (GFP-labeled cells could not be grown under minimal media conditions due to the selective pressure of the antibiotics needed to maintain the plasmid). The P values associated with the zeta potential comparisons (based on Univariate ANOVA test) between different experimental treatments are presented in Table 7 and Table 8.

Table 7: P-values of zeta potential comparisons of different bacterial species exposed to the same environmental states and growth conditions. Numbers with asterisk represent significant differences based on the Univariate ANOVA Test (P≤ 0.05).

Bacteria Type	**Medium**	**Bacteria Type**		
		***E. coli* + GFP**	***Salmonella***	***Pseudomonas***
E. coli	Rich	0.683	0.000*	0.845
	Minimal		0.000*	0.127
	Starved	0.054	0.000*	0.227
	Dead	0.635	0.000*	0.533
E. coli + GFP	Rich		0.000*	0.819
	Starved		0.000*	0.393
	Dead		0.000*	0.533
Salmonella	Rich			0.000*
	Minimal			0.000*
	Starved			0.000*
	Dead			0.000*

Table 8: P-values of zeta potential comparisons for the same species of bacteria exposed to different environmental states and growth conditions. Numbers with asterisk represent significant differences based on the Univariate ANOVA Test (P≤ 0.05).

Medium	Bacteria Type	Medium		
		Minimal	**Starved**	**Dead**
Rich	*E. coli*	0.121	0.014*	0.497
	E. coli + GFP		0.579	0.726
	Salmonella	0.004*	0.009*	0.962
	Pseudomonas	0.9895	0.119	0.248
Minimal	*E. coli*		0.213	0.596
	Salmonella		0.722	0.007*
	Pseudomonas		0.117	0.246
Starved	*E. coli*			0.037*
	E. coli + GFP			0.848
	Salmonella			0.016*
	Pseudomonas			0.672

BACTERIAL SIZE MEASUREMENTS

The bacterial cell sizes were measured to understand the effects of exposing cells to different nutrient levels as well as to understand their influence on the electrophoretic mobility. Sizes were measured by imaging the cells using Differential Interference Contrast Microscopy (DICM).

The images were acquired on a Zeiss Axiophot (Carl Zeiss Microimaging, Thornwood, NY) microscope using a 100x/1.3 oil immersion objective, a 1.4 NA oil immersion condenser and a Coolsnap CF (Photometrics, Tucson, AZ) digital camera controlled by MetaVue software v.5 (Molecular Devices Corporation, Downingtown, PA). The images were spatially calibrated and the lengths of the bacterial cells were measured manually using ImageJ software [74]. Images were generated at the Microscopy and Imaging Center at Texas A&M University. A cover slip was used on top of the cell samples to ensure that the cells were uniformly flattened on the slide surface so that they were aligned along one single plane. Around 20 images of each bacterial sample were taken and the lengths of 97 to 100 individual bacterial cells were measured and averaged. Representative images of *E. coli* suspended in drinking water cultured in different growth media are presented in Figure 3. Table 9 represents the size distributions of the different bacterial cells along with the corresponding *P* values [75] for test of normality of the distribution.

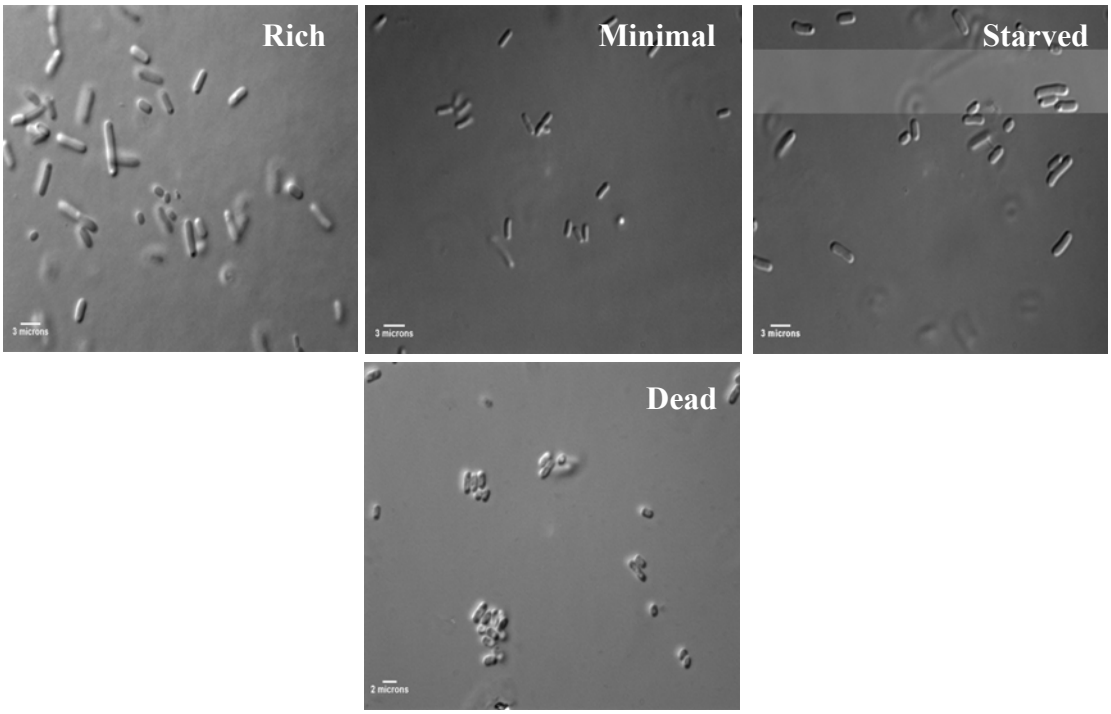

Figure 3: Differential Interference Contrast Microscopy (DICM) images of *E. coli* cells grown in different nutrient conditions suspended in drinking water.

Table 9: Size distributions of different bacterial cells under various physiological conditions, and test of normality of bacterial lengths as determined by the Kolmogorov-Smirnov Test. Size distribution: Mean values ± standard deviation (n= between 97 and 100 images) Normality test: The *P* value was used for comparisons. Numbers with asterisk represent normal distribution based on the Kolmogorov-Smirnov Test for normality (P > 0.05).

Bacteria (state)	Cell size (μm)	Degrees of Freedom	*P* Value
E. coli (rich)	3.3 ± 0.9	100	.013
E. coli (minimal)	2.6 ± 0.6	100	.000
E. coli (starved)	3.2 ± 0.8	100	.007
E. coli (dead)	2.3 ± 0.5	100	.038
E. coli + *GFP* (rich)	3.8 ± 0.9	100	.200*
E. coli + *GFP* (minimal)	2.9 ± 0.7	100	.007
E. coli + *GFP* (dead)	2.8 ± 0.5	100	.200*
Pseudomonas (rich)	2.1 ± 0.6	97	.005
Pseudomonas (minimal)	1.7 ± 0.3	97	.077*
Pseudomonas (dead)	1.7 ± 0.4	97	.200*
Salmonella (rich)	2.2 ± 0.3	97	.200*
Salmonella (minimal)	1.7 ± 0.3	97	.200*
Salmonella (starved)	1.8 ± 0.4	97	.040
Salmonella (dead)	1.5 ± 0.3	97	.042

There were visible differences in shape among different bacteria as well as between the different treatments (Figure 3). The bacterial cells when grown in rich medium ranged from 2.1 μm to 3.3 μm in length. Unlabeled *E. coli* cells were smaller

than the GFP-labeled *E.coli* cells under all three (rich, starved and dead) conditions (Table 2). The cells grown under minimal media conditions ranged from 1.7 µm to 2.9 µm, while the starved cells ranged in length from 1.8 µm to 3.2 µm. The size distributions of *E. coli* grown under different media conditions are presented in Figure 4.

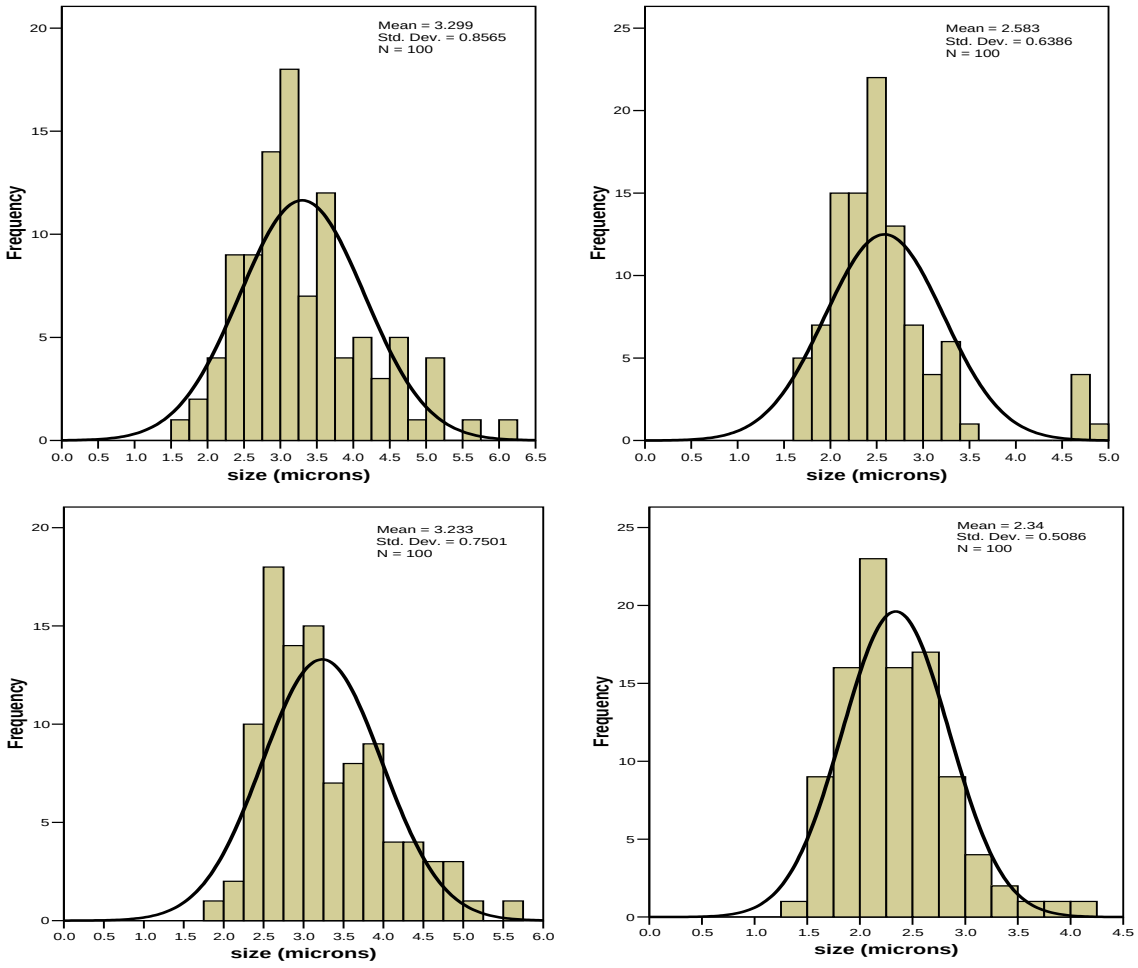

Figure 4: Size distributions of *E. coli* cells in different environmental states and growth conditions.

It can be seen from this figure that not all cell preparations were normally distributed. The rich medium *E. coli* cells distribution follows the trend observed by Kilian et al. (size range between 1 μm - 4 μm) [76].

DISCUSSION

There are previous reports indicating that cells when grown under different nutrient conditions would exhibit differences in size and shape. The conversion of rod-shaped cells to spherical shapes has long been considered one of the survival strategies of bacteria in the environment [77-80]. Our results suggest that there are significant variations in cell sizes among closely related enteric bacteria even under starvation and minimal media conditions (Figure 3 and Table 9). These findings can be relevant when attempting to use analytical instruments such as flow cytometry and coulter counter instruments for detecting and enumerating cells in suspensions. Similarly, the configuration in which bacterial cells attach to surfaces could be significantly different from what is predicted depending on the relative concentrations of spherical and rod-shaped cells. A previous laboratory study using polystyrene beads have shown that *E. coli* generally attach to surfaces based on charges concentrated at specific ends of the bacterial cell [81].

Previous studies demonstrating the use of capillary electrophoresis to elucidate bacterial zeta potentials utilized laboratory prepared buffer solutions, and for the most part, these studies have used bacterial cells grown in typical “rich” laboratory media. The present study is unique in that it has employed different bacterial genera grown or exposed to different nutrient conditions to simulate different environmental states of

bacterial cells and their zeta potential was determined in realistic drinking water environments. The measured electrophoretic mobility of *E. coli* across the different physiological conditions ranges from -3.13 *μm-cm/V-sec* to -3.8 *μm-cm/V-sec*, which is in the same range reported in previous studies by Hayashi et al [82] using similar ionic strength buffers and similar pH conditions. Lytle et al. [83] have shown the mobility of *E. coli* to be around -1 *μm-cm/V-sec* using buffers with ionic strengths similar to the one used in this study. However, the difference in mobility between our measurements and Lytle et al. arises from the fact that the pH of their buffer was around 6 whereas the pH of the drinking water used in this study was 8.4. It has been shown [35, 83] that the electrophoretic mobility increases with increasing pH for a particular ionic strength. Therefore, our mobility measurements follow the trend predicted in the literature.

From the size measurements, it was seen that the GFP-labeled *E. coli* were larger than the unlabeled *E. coli* (Table 9). The data also suggests that with GFP, cell size is not significantly influenced even when the cells are dead (Table 9). These results suggest that the cloning of genes encoding intracellular proteins actually cause an increase in cell dimensions whose electrophoretic mobility does not decrease even when the cells die. The finding that dead cells have altered zeta potentials can also have implications on biofilm stability under nutrient limited conditions and bacteriocidal agents [84-86].

The present study is significant in that it is the first report demonstrating that municipal drinking water can be used as the buffer in capillary electrophoresis and it opens up the possibility of using CE measurements to predict the surface charges of bacterial cells exposed to different conditions in drinking water. Based on the zeta

potential measurements, the charge distribution in the overlapping double layer between the bacterial cell surface and the substratum surface can be estimated. This relates directly to the electrostatic interactions of colloidal adhesion to solid substrata as described by the DLVO theory. Knowledge of these interactions can enable us to device different methodologies to reduce bacterial adhesion, or in cases where adhesion occurs, altering the chemistry of the substratum surface by adding surfactants coupled with external mechanisms like shear force and/or electrokinetic forces could be used to reverse bacterial adhesion. The zeta potential measurements are used to design the microfluidic based concentration device to be unspecific to microorganism type.

DESIGN AND FABRICATION OF SINGLE CHANNEL PROTOTYPE DEVICE

INTRODUCTION

Developing a continuous, species non-specific capture system requires careful consideration of the various time scales involved in particle motion due to electric field, and fluid motion due to the external pressure gradient. Particle migration time (time taken for particle to migrate to anode) and residence time (time of particle residence in channel based on external flow) are essential in device optimization. Smaller residence times result in shorter channels, which minimizes the device wetted volume, pumping and electrical power. The voltage applied during capture is limited by the electrolysis potential of water (1.23 V) to avoid bubble formation in the channels. In addition, electrochemical effects have to be considered in DC electric fields. Since the applied electric potential is limited, large electric fields can be obtained by reducing the electrode spacing, which is the critical design parameter. Biocompatibility issues and electrochemistry between the electrode and the ionic media needs to be considered while choosing an appropriate electrode material.

The microfluidic device is intended to sample large volumes of water, and sufficiently concentrate them down to smaller volumes compatible with current and future detection technologies. Hence, it is critical to ensure that the wetted volume of the device is as small as possible. This ensures high levels of concentration within reasonable time frames. Also, the device is meant for sampling water in recycled water

systems in space stations, as well as various terrestrial applications. Hence, the power consumption (electrical and mechanical pumping power) needs to be minimized in order to make it useful and efficient for real-time field applications. In this section, we present the various design constraints and physical design limits that were considered before choosing the dimensions of the single channel prototype device. Particularly, the wetted volume and power of the device are minimized. Flow in the channel is modeled using Poiseuille flow relations to predict various time scales involved in particle motion.

MICROFLUIDIC DEVICE DESIGN AND PRINCIPLE OF OPERATION

The microfluidic device consists of two parallel electrodes of length *L* and width *W* separated by a distance *h* (Figure 5).

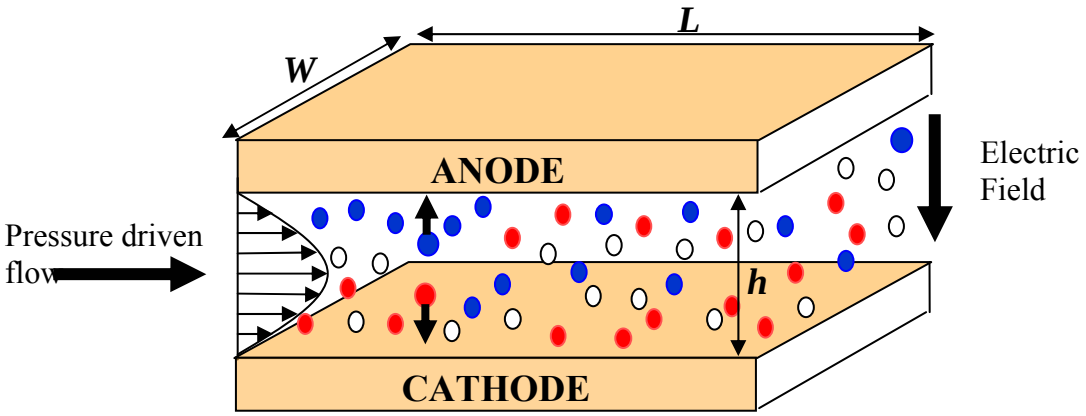

Figure 5: Schematic of single channel microfluidic device.

Pressure driven flow is applied through the channel to maintain the flow, while a constant potential difference between the electrodes creates a uniform electric field (E). This generates a configuration similar to capacitor plates with electrodes forming the channel walls for microorganism adhesion. Under the uniform electric field, negatively charged particles travel towards the anode with constant electrophoretic velocity (V_{EP}), represented as

$$V_{EP} = \mu_{EP} E \,, \tag{7}$$

where μ_{EP} is the electrophoretic mobility of microorganisms. Applied electric field and channel height are the two critical design parameters that dictate particle motion towards the anode. Based on the electrophoresis concept, time required for particle migration towards the anode can be predicted as

$$t_M = \frac{h}{V_{EP}} \,. \tag{8}$$

In order to assure efficient particle capture, the electrophoretic particle migration time (t_M) must be less than the particle residence time (t_R) in the channel, which can be predicted as

$$t_R = \frac{L}{V_{AVE}} \,, \tag{9}$$

where V_{AVE} is the average velocity of flow in the channel. For pressure driven flows, the maximum flow velocity happens in the middle of the channel, and its magnitude is 1.5 V_{AVE}. Therefore, $t_M/t_R << 1$ is a critical design constraint in selection of the channel dimensions, applied electric field and the flowrate. We utilized the smallest

electrophoretic mobility value of -0.31 μm-cm/V-sec from Table 5, which results in $t_M \approx$ 10 s. This ensures efficient capture of even the slowest moving microorganisms, before they leave the channel. Therefore, the capture device design is generic to a large range of microorganisms with various mobilities.

Particle residence time (t_R) is essential in device optimization. Smaller residence times result in shorter channels, which minimizes the device wetted volume, pumping and electrical power. The voltage applied during capture is limited by the electrolysis potential of water (1.23 V) to avoid bubble formation in the channels. In addition, DC electric fields may lead to electrochemical effects, resulting in pH gradients and current fluctuations in the system [87]. Under pH gradients, bacteria move to their isoelectric point, as opposed to migrating towards the electrode [19]. Flow through the channel reduces diffuse charge dynamics effects reported in [87], and steadily maintains substantial currents to induce electrophoretic motion (Table 10). In addition, voltages smaller than the electrolysis potential of water reduces the pH gradients and fluctuations. Since the applied electric potential is limited, large electric fields can be obtained by reducing the electrode spacing (h), which is the critical design parameter.

Another critical design issue is the electrode material. Gold, palladium, platinum and titanium etc., are inert and biocompatible. Electrochemistry between the electrode and the ionic media needs to be considered while choosing an appropriate electrode material. The electric potential that can be applied without contaminating the electrode is limited by the electrode oxidation potential at which the metal starts reacting with water. Finally, the electrode material should also be machinable. Considering all of the above

factors, we chose gold coated glass slides as the electrode material, since the oxidation potential of gold is around 1.6 V, which is less than the electric potentials applied in this study (1.0 V, 1.25 V). In addition, gold is a noble metal and it is biocompatible. Toxicity of gold to the microorganisms was also tested. We were able to successfully recover the bacteria after 3 to 4 hours of contact between the bacteria and gold surfaces using culture based methods. Hence, the bacterial cells were not killed and/or did not become viable but unculturable.

Fluid flow in the channel can be characterized as two-dimensional, fully developed, pressure driven laminar flow. Large channel aspect ratio ($h/W<<1$) maintains mostly two-dimensional flow in the system, and the Reynolds number based on the channel height is about 0.02. Therefore the flow is in the Stokes regime, and the flow development length (at the entry of the channel) is negligible compared to the channel length (L) [88]. For a given volumetric flowrate ($\dot{Q}$), the average channel velocity is

$$V_{AVE} = \frac{\dot{Q}}{Wh}. \tag{10}$$

The pressure drop in the channel can then be found as [88]

$$\Delta p = \frac{12\dot{Q}\eta L}{Wh^3}, \tag{11}$$

where η is the absolute viscosity. Pressure drop is important for estimating the pump power required to drive the flow, and also for calculating the shear stress on channel walls. The latter is important to quantify the shear force experienced by the cells stuck

on channel walls. For a specified pressure drop, shear stress on the channel surfaces can be predicted by [88]

$$\tau = \frac{h\Delta p}{2L} \tag{12}$$

The microfluidic channel dimensions were chosen to minimize the power required to pump fluid into the channel ($P_{pump} = \dot{Q} \times \Delta p$) and the wetted volume ($\forall = LWh$) of the channel at the same time. Figure 6 represents the design plot (pumping power and wetted volume) for the microfluidic device, as a function of channel hydraulic diameter.

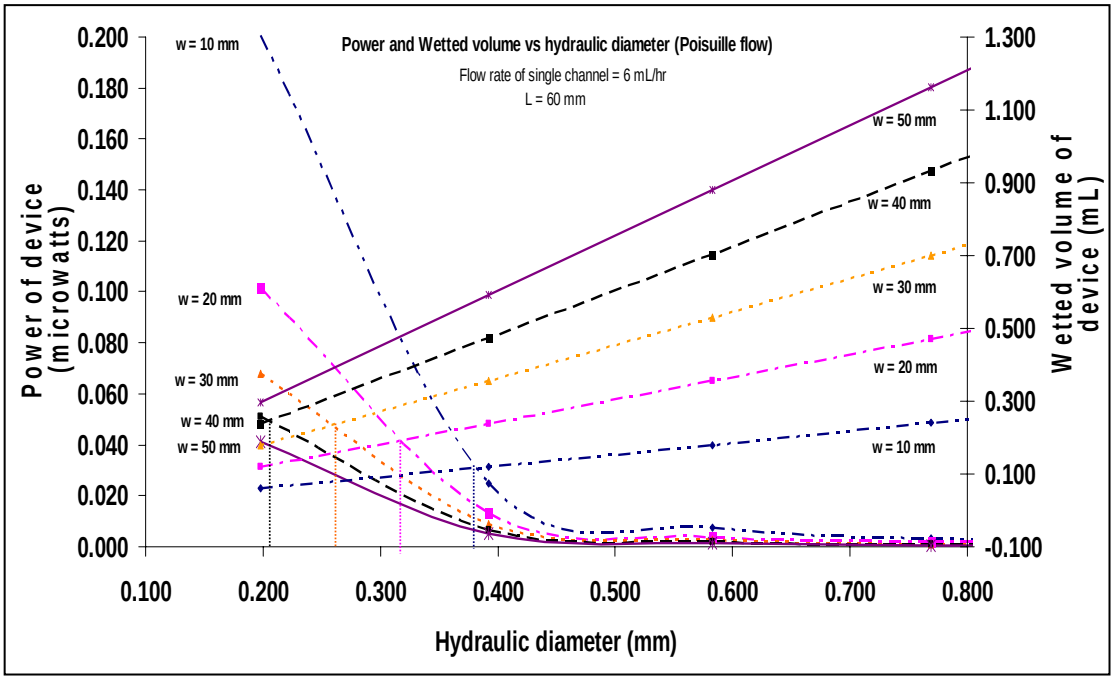

Figure 6: Design plot of wetted volume and pumping power of single channel as a function of channel dimensions.

To generate the above plot, the length of channel was assumed to be 60 mm, based on physical constraints, and to satisfy the design constraint of $t_M/t_R << 1$. In Figure 6, the intersection point of wetted volume and power for different channel widths represents a design point (minimal wetted volume and power). Considering these design points, along with other design and physical constraints mentioned previously, the channel dimensions were chosen to be 60 *mm* (*L*) × 40 *mm* (*W*) x 150 μm (*h*). Table 10 presents critical parameters for the microchannel design, including channel dimensions, particle time scales, electric field and current, and the electric and mechanical power.

Table 10: Critical parameters of the single channel prototype microfluidic device.

Device Parameter	Value
Device Dimensions	60 *mm* (*L*) X 40 *mm* (*W*) x 150 μm (*h)*
Channel wetted volume (ml)	0.36 *mL*
Particle migration time based on smallest mobility	~ 10 *s*
Particle residence times	10.8 *min* (2 *mL/hr)*, 5.4 *min* (4 *mL/hr)*, 3.6 *min* (6 *mL/hr)*
Applied potential differences and electric fields	1.0 *V* (6.7 *V/mm*) and 1.25 *V* (8.4 *V/mm*)
Steady electric current in the system	20 μA (1.0 V), 26 μA (1.25 V)
Electrical power consumption per channel	20 μW (1.0 *V)*, 32 μW (1.25 *V)*
Pressure drop from equation (6)	2.97 *Pa* (2 *mL/hr*), 5.94 *Pa* (4 *mL/hr*), 8.91 *Pa* (6 *mL/hr*)
Pumping power	1.65 *nW* (2 *mL/hr*), 6.60 *nW* (4 *mL/hr*), 14.85 *nW* (6 *mL/hr*)

MICROFLUIDIC DEVICE FABRICATION

The microfluidic channel walls (anode and cathode) were fabricated from 50 *mm* × 75 *mm* plain glass slides by coating them with 99.99% pure gold (35 nm thickness). A barrier layer of chromium (15 nm) was used between the glass and gold since gold does not directly adhere to glass. Both chromium and gold deposition on glass were done in a high vacuum metal deposition chamber (BOC Edwards Auto 306 metal evaporation chamber) at a deposition rate of 0.05 nm/s. Prior to deposition, the glass slides were cleaned thoroughly by rinsing with acetone, isopropanol and millipore filtered deionized water for 2 minutes for each process. This enables deposition of a uniform layer of gold on the glass. Also, prior to the gold deposition, holes for inlet and outlet were drilled on the glass slide to be used as anode. Teflon tubing with 0.87 *mm* inner diameter was used for inlet and outlet tubing.

The spacing between electrodes was created using a 150 μm thick double sided adhesive tape (Removable double sided adhesive, 3M corp.). The top and bottom electrodes were misaligned by 5 mm along the length to create the necessary spacing for electrical wiring. The wires were glued to the electrodes using silver epoxy (Stan Rubinstein Associates). After the assembly, a microchannel with dimensions of 60 mm × 40 mm × 150 μm was obtained. The channel was sealed with epoxy from the outside to eliminate leaks in the system. Figures 7 and 8 show a schematic of the assembly process and a picture of the assembled microfluidic device respectively.

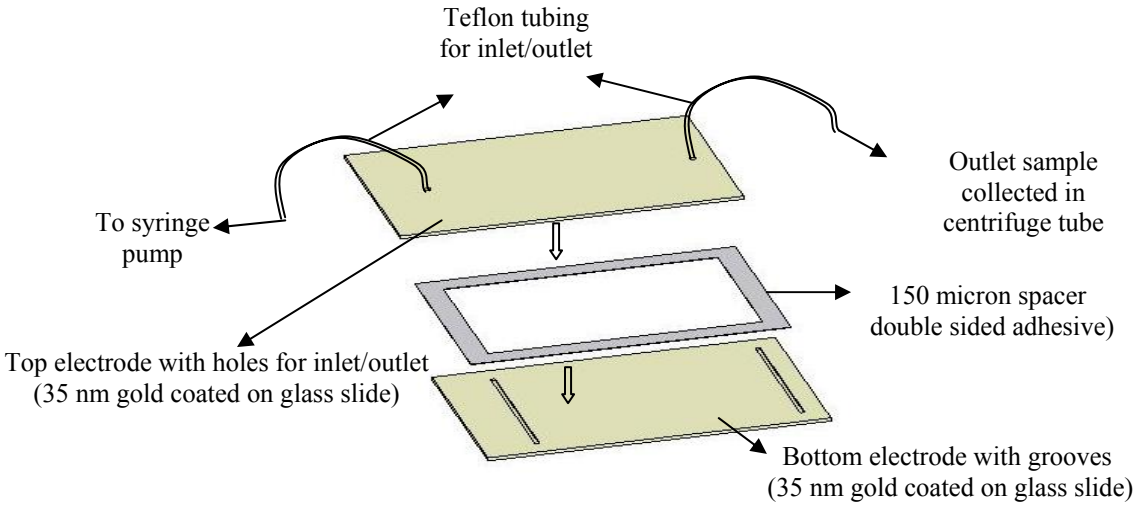

Figure 7: Schematic of microfluidic device assembly.

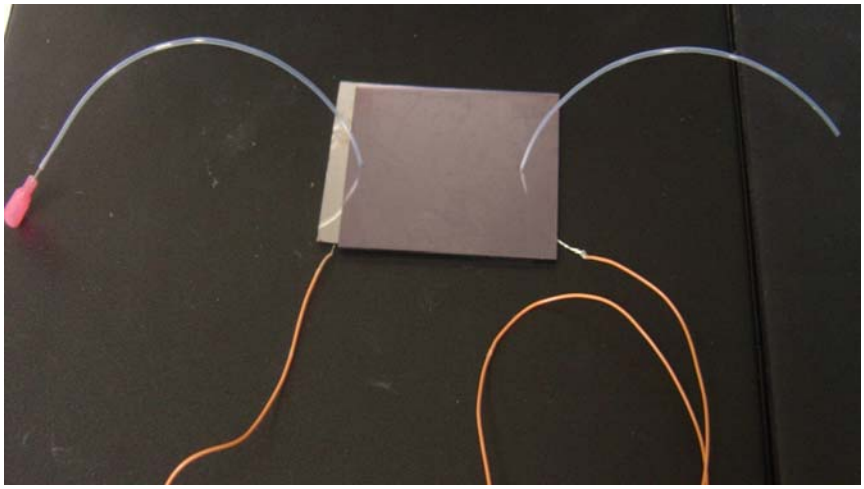

Figure 8: Picture of Assembled Single Channel Prototype Microfluidic Device.

TESTING OF SINGLE CHANNEL PROTOTYPE MICROFLUIDIC DEVICE FOR EFFICIENCY – PLATING AND REAL-TIME PCR

INTRODUCTION

Three different methods were employed for testing the single channel prototype microfluidic device performance. These include indirect methods of quantification like plating and real-time PCR, and direct observation of capture on the anode by performing particle tracking using fluorescent microscopy. In this section, we discuss the methods and protocols employed for quantifying the capture efficiency of the single channel prototype device based on culture based methods like plating along with validation studies using molecular methods like real-time PCR. The performance of the device is analyzed as a function of channel flow rate, applied electric field, and pH and ionic strength of the suspending media. The concentration factors that are achieved with the single channel prototype device at different flow rates are presented. Finally, comparison of the power requirements between the microfluidic device developed in this study and existing concentration methods is also presented.

CULTURING OF STRAINS AND QUANTIFICATION PROCEDURES

Microorganisms

E. coli DH5α, *Pseudomonas sp.*, and *Salmonella* Newport and two viruses (*MS-2* and Echovirus 11 -ATCC # VR-1052) were used in this study. *E. coli* DH5α and *Salmonella* Newport and *Pseudomonas sp* were grown at 37ºC in unamended Luria-Bertani (LB) broth and tryptic soy broth (TSB) respectively. The cells (30 mL) were

centrifuged (3300 × *g)* and washed 3X using 10 mL of filter sterilized water. The washed cells were then resuspended in 40 mL of fresh filter sterilized water for experimentation. The cells were quantified by plate counts to ensure a concentration of approximately 10^6 CFU/mL. The samples were tested in the microfluidic device within 4-6 hours of preparation.

Viruses

E. coli Famp strain was used as a host to prepare a high titer (10^6 PFU/mL) lysate using the double agar overlay method based on previously published protocols [89]. For *Echovirus 11*, BGMK kidney cells were employed to prepare a lysate containing approximately 10^6 PFU/mL [89].

Quantification Using Plating

Three different dilutions of each sample (three replicates each) from the microfluidic device were prepared in phosphate buffer. Ten (10 μL) of sample mixed with 90 μL of phosphate buffer were plated on LB agar (*E. coli* DH5α and *Salmonella* Newport) and TSA (*Pseudomonas* sp.) and incubated for 16-18 hrs at 37 ºC prior to enumeration. The colonies were counted and averaged to quantify the concentration of cells in the original sample. The double agar overlay procedure was used to enumerate the *MS2* phages in the samples. Quantification of the *Echo* viruses was performed using the method used by Vega et al. [89] and results were expressed as PFU/mL.

Quantification Using Real-time PCR

A commercially available AOAC validated real-time PCR assay based on molecular beacon technology (Genevision™ real-time PCR system, Warnex Inc. Quebec

City, Canada) was used for quantitative detection of *Salmonella* sp. using real-time PCR. The protocol used for real-time PCR amplification was as follows. In the first step, 10 μL of samples (three replicates each) were mixed with 90 μL of the extraction buffer in a microtiter plate. The extraction plate provided by the manufacturer was run at 90 ºC for 15 minutes to lyse out the DNA from bacterial cells. Later, the microtiter plate with extracted DNA was centrifuged at 1800 × g for 5 minutes to sediment cell debris. Following this, 10 μL of extracted DNA sample was collected from the top of the extraction plate and mixed in another microtiter plate (detection plate) containing 15 μL of detection buffer, which was also provided by the manufacturer. The detection plate was then placed on the thermocycler, and the instrument was run for 40 PCR cycles (melting at 95 ºC for 1 minute, annealing at 57 ºC for 1 minute and extension at 72 ºC for 1 minute). Fluorescence measurements at the end of each cycle were recorded real-time and amplification plots were obtained using the Sentinel software (Genevision™ System).

A standard curve was generated to determine the number of target organisms present in the original sample. Different dilutions of standard samples (10^1 – 10^6 CFU/mL), with cell counts (known earlier by plating) were included as part of the samples and were analyzed along with each PCR assay. The number of cycles, after which a significant shift in fluorescence is observed, is denoted as the threshold value (Ct value) for each sample. The Ct value of each sample analyzed in the PCR reaction is a linear function of the amount of target DNA in the original sample [log (CFU/ml)]. A calibration curve was generated between the Ct values and the log (CFU/mL) of the

standard samples with known cell counts. Since the slope and intercept of this graph are similar for the standard and unknown samples, the Ct values of the unknown samples were used along with the slope and intercept of the standard calibration curve to find the actual cell count in each sample. Each sample was run in triplicates to obtain a measure of the average cell count.

SURVIVAL STUDIES WITH GOLD ELECTRODE

Survival studies were performed with the gold electrodes to ensure that exposure to gold did not kill or induce the viable but non culturable state (VBNC) in microorganisms. *E. coli* DH5α strain was used for this study. The cell suspension was prepared in recycled water at concentrations of ~ 10^7 CFU/mL and exposed to the electrode for three hours by spreading a 100 μL droplet on the surface. The cells were then recovered and plated to compare the concentrations prior to and after exposure to gold for three hours. This procedure was repeated three times. The initial concentration of the bacterial cells prior to exposure to gold was 4.5×10^8 CFU/mL. After exposure to gold for 3 hours, the concentration of the cells was 2.5×10^8 CFU/mL. Hence, the bacterial cells were not killed and/or did not become viable but unculturable.

EXPERIMENTAL SETUP AND DATA ANALYSIS

Microorganism capture experiments were performed for *E. coli, Salmonella, Pseudomonas*, *MS-2* and *Echovirus* at potential differences of 1.0 and 1.25 V, and at flow rates of 2, 4 and 6 mL/hr. All experiments were carried out using an initial concentration of ~10^6 CFU/mL in the case of bacterial cells, and ~10^6 PFU/mL in the case of viruses. Lower initial concentrations, representative of potable water numbers,

could not be used, because, the cells collected at the device outlet, would then be below the sensitivity thresholds of the culture based and real-time PCR detection assays.

Two identical devices were tested in parallel to quantify the efficiency of capture. Microorganism capture occurs at the anode of the device that has the electric field turned on. The second device experiences zero electric field, and was used for negative control. Hence, the negative control device was used to account for any organisms that may be captured in the inlet/outlet tubing or any other device accessories. While calculating the device capture efficiency, negative control was used as the reference sample to negate the aforementioned effects. Both devices were connected to the same syringe pump dispensing microorganism samples at a constant flow rate. Hence, the capture and negative control devices used the same inlet sample for consistency. The samples from outlet tubes of both devices were collected in a microcentrifuge tube for analysis. Each experiment was repeated atleast three times. A standard protocol was used for running each experiment in terms of device rinsing procedure, experimental conditions, time of experiment, and sample handling. This ensures that these experiments are highly reproducible. Figure 9 represents a schematic of the experimental setup used in this study.

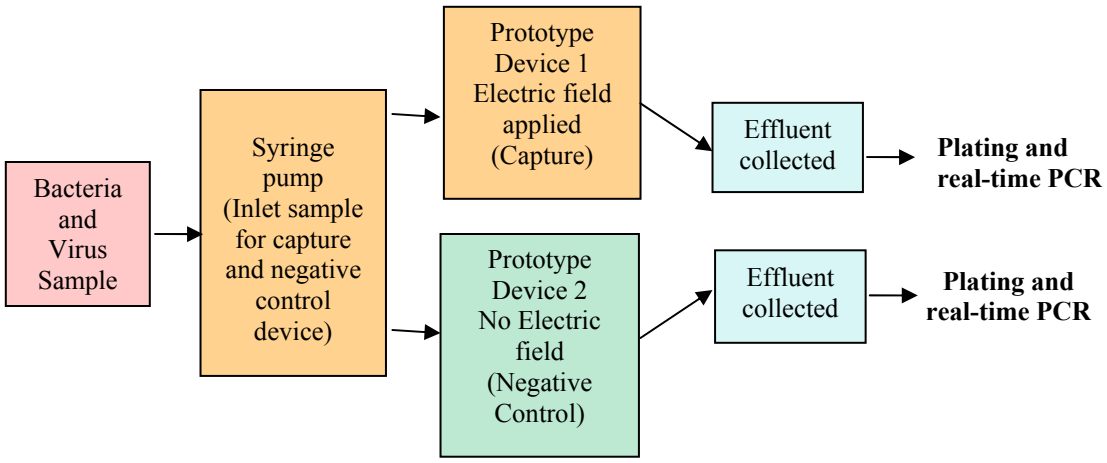

Figure 9: Schematic of experimental setup for plating and PCR experiments.

Samples collected from the outlet of both capture and negative control devices were analyzed for cell counts using culture based methods and real-time PCR assays. The CFU/ml of outlet samples of the capture [$\theta_{Cap(Plate)}$] and negative control [$\theta_{NC(Plate)}$] devices are obtained by plating, and the efficiency of microorganism capture based on plating is calculated using

$$\eta_{Plate} = \left(\frac{\theta_{NC(Plate)} - \theta_{Cap(Plate)}}{\theta_{NC(Plate)}} \right) \times 100\% . \qquad (13)$$

Similarly, the CFU/ml of outlet samples of the capture [$\theta_{Cap(PCR)}$] and negative control [$\theta_{NC(PCR)}$] devices are obtained using real-time PCR, and the efficiency of microorganism capture based on real-time PCR is calculated using

$$\eta_{PCR} = \left(\frac{\theta_{NC(PCR)} - \theta_{Cap(PCR)}}{\theta_{NC(PCR)}} \right) \times 100\% . \quad (14)$$

It must be emphasized that since the capture efficiencies were calculated using the negative control sample as opposed to the inlet sample, these efficiencies reflect capture as a result of the electric field only. Prior to the quantification, cell viability assays using *Bac*Light™ Bacterial Viability Kits (Invitrogen) were performed to ensure that the applied electrical potential was not inactivating the cells (data not included).

RESULTS AND DISCUSSION

Pathogen capture experiments were performed for *E. coli, Salmonella, Pseudomonas*, *MS-2* and *Echovirus* at potential differences of 1.0 and 1.25 V, and at flow rates of 2, 4 and 6 mL/hr. All experiments were carried out using an initial concentration of ~10^6 CFU/mL in the case of bacterial cells, and ~10^6 PFU/mL in the case of viruses. Tables 11 and 12 highlight the capture efficiencies of *E. coli*, *Salmonella* and *Pseudomonas* from NASA reclaimed water using electric potential difference of 1.0 V (E = 6.7 V/mm) and 1.25 V (E = 8.4 V/mm), respectively. The flow rate for these experiments was 2 mL/hr. The cells collected at the outlet of both the negative control and capture device were quantified using plating.

Table 11: Capture efficiency of bacterial cells from recycled water at 1.0 V potential drop and at 2 mL/hr (E = 6.7 V/mm, Inlet concentration of cells ~ 10^6 cfu/ml).

Time	***Salmonella*** **2 ml/hr Plating (%)**	***E. coli*** **2 ml/hr Plating (%)**	***Pseudomonas*** **2 ml/hr Plating (%)**
t = 15 mins	90.2 ± 9.5	91.3 ± 4.3	92.9 ±6.6
t = 30 mins	96.1 ± 3.8	95.7 ± 2.2	98.1 ± 1.5
t = 45 mins	90.6 ± 9.1	85.4 ± 9.3	94.3 ± 4.8
t = 60 mins	85.5 ± 14.4	92.1 ± 6.6	82.8 ±13.9

Table 12: Capture efficiency of bacterial cells from recycled water at 1.25 V potential drop and at 2 mL/hr. (E = 8.4 V/mm, Inlet concentration of cells ~ 10^6 cfu/ml).

Time	***Salmonella*** **2 ml/hr Plating (%)**	***E. coli*** **2 ml/hr Plating (%)**	***Pseudomonas*** **2 ml/hr Plating (%)**
t = 15 mins	99.996 ±0.003	99.7 ±0.2	98.6 ± 0.9
t = 30 mins	99.997 ± 0.001	99.8 ± 0.1	99.6 ± 0.2
t = 45 mins	99.997 ± 0.004	99.4 ± 0.4	99.7 ± 0.3
t = 60 mins	99.998 ± 0.002	98.7 ± 1.1	99.2 ± 0.8

It can be seen from Table 11 that using a potential drop of 1.0 V, there is one to two log reduction in the number of cells at the outlet, compared with the negative control

experiment. The capture efficiencies presented in this table were calculated from the cell counts using equation (13). Capture efficiencies as high as 90% were achieved within 15 minutes of operation of the device. It should also be noted that the capture efficiency is independent of the bacterial cell type. For all bacterial types, the maximum efficiency of capture was achieved after 30 minutes. The efficiency seems to reduce slightly at later times. Three to four logs of reduction in the number of cells at the device outlet were observed at 1.25 V (Table 12). In addition, the capture efficiencies remain consistent during the one hour sampling period. Since these results are obtained during a flow process, there is continuous accumulation of captured cells on the electrode surfaces. We must point out that the capture efficiencies would be higher, if inlet samples were used as the reference for calculation, instead of the negative control device data.

Table 13 presents the capture efficiency of *Salmonella* cells from reclaimed water, three leading brands of bottled water and 1 mM phosphate buffer (pH=5.5) using electric potential difference of 1.25 V (8.4 V/mm) and 2 mL/hr flow rate. Quantification for this set of experiments was performed using plating. The pH and ionic strength of the different media used in this set of experiments was presented in Table 3.

Table 13: *Salmonella* capture efficiency from bottled and recycled water and phosphate buffer at 1.25 V potential drop and at 2 mL/hr. (E = 6.7 V/mm, Inlet concentration of cells ~ 10^6 cfu/ml).

Time	*Salmonella* 2 mL/hr				
	Bottled Water 1 (%)	**Bottled Water 2 (%)**	**Bottled Water 3 (%)**	**NASA Reclaimed Water (%)**	**Phosphate buffer (%)**
t = 15 mins	96.6 ± 1.5	95.6 ± 4.4	94.0 ± 0.9	99.996 ±0.003	99.98 ± 0.01
t = 30 mins	98.3 ± 0.8	98.3 ± 1.7	95.6 ± 1.5	99.997 ± 0.001	99.97 ± 0.02
t = 45 mins	98.7 ± 0.4	97.9 ± 2.1	98.1 ± 0.3	99.997 ± 0.004	99.20 ± 1.83
t = 60 mins	98.1 ± 1.4	96.4 ± 3.6	96.6 ± 0.2	99.998 ± 0.002	97.03 ± 3.84

Bottled water and phosphate buffer experiments resulted in 94% to 99% capture efficiencies, while capture efficiency from recycled water was consistently at 99.99% and higher. This discrepancy could be attributed to the differences in ionic strengths of bottled and recycled waters (Table 3). Higher ionic concentrations (bottled water) result in thinner electric double layers, which affect electrostatic interactions as described by the DLVO theory [6, 32]. In the case of thinner EDL, the cells have to get in much closer proximity to the surface, to have higher electrostatic attraction from overlapping double layers. Hence, within the time frames tested, capture for recycled water, which has thicker EDL is higher, because the electrostatic interactions are more attractive even at

larger cell-surface distances, when compared to bottled water and phosphate buffer experiments.

Salmonella sp. cells captured from reclaimed water were also quantified using real-time PCR. The PCR analysis ensures that dead cells, viable but unculturable cells, and naked DNA, which could not be quantified using the culture based methods, are also accounted for. Table 14 presents a comparison between the capture efficiencies calculated using equations (13) and equation (14), based on the plate counts and real-time PCR cell counts, respectively.

Table 14: Comparison of *Salmonella* capture efficiency between plating and real-time PCR from recycled water at 1.0 V potential drop and at 2 and 4 mL/hr. (E = 6.7 V/mm, Inlet concentration of cells ~ 10^6 cfu/ml).

	Salmonella			
	2 ml/hr		**4 ml/hr**	
Time	**Plating**	**PCR**	**Plating**	**PCR**
t = 15 mins	90.2 ± 9.5	67.6 ± 1.7	94.83	46.77
t = 30 mins	96.1 ± 3.8	66.3 ± 1.6	98.17	46.77
t = 45 mins	90.6 ± 9.1	44.2 ± 1.3	97.96	71.68
t = 60 mins	85.5 ± 14.4	42.2 ± 2.1	97.96	31.74

Table 14 shows that real-time PCR capture efficiencies are lower than the plating capture efficiencies at all times. This mismatch can be explained as follows: Culture based methods like plating quantify only the culturable cells. However, real-time PCR accounts for culturable, viable but unculturable and dead cells, as well as the naked DNA. Hence, when Equation (13) is used to calculate the device capture efficiency based on plating, $\theta_{Cap(Plate)}$ and $\theta_{NC(Plate)}$ take only the culturable cells into account. When Equation (14) is used to calculate the device capture efficiency based on real-time PCR, in addition to the culturable cells, both $\theta_{Cap(PCR)}$ and $\theta_{NC(PCR)}$ account for the dead cells, naked DNA and viable but unculturable cells. Due to this reason $\theta_{NC(PCR)} > \theta_{NC(Plate)}$ and $\theta_{Cap(PCR)} > \theta_{Cap(Plate)}$, which primarily affects the denominator of Equations (13) and Equation (14), and results in $\eta_{PCR} < \eta_{Plate}$.

Table 15 presents the capture efficiency at four different flow rates (2, 4, 6 and 9 ml/hr) for *Salmonella* cells at 1.0 V. Quantification for this set of experiments was performed using plating.

Table 15: *Salmonella* capture efficiency comparison at different flow rates using plating (E = 6.7 V/mm, Inlet concentration of cells ~ 10^6 cfu/ml).

Time	*Salmonella*			
	2 ml/hr Plating	4 ml/hr Plating	6 ml/hr Plating	9 ml/hr Plating
t = 15 mins	90.2 ± 9.5	98.1 ± 1.7	99.5 ± 0.3	33.38
t = 30 mins	96.1 ± 3.8	97.5 ± 1.6	90.9 ± 7.3	38.00
t = 45 mins	90.6 ± 9.1	90.7 ± 8.1	72.2 ± 22.7	33.62
t = 60 mins	85.5 ± 14.4	87.6 ± 11.4	78.3 ± 17.3	45.13

It can be observed from Table 15 that the device capture efficiency is consistently around 90-99% at 4 mL/hr flow rate for one hour operation. However, at 6 mL/hr, the capture efficiencies drop to around 70-80% beyond 30 minutes. At 9 mL/hr, the capture efficiencies were quite low. This can be attributed to lower particle residence times (2.4 min) predicted by equation (9). Therefore, the majority of particles leave the channel before they can be captured.

Table 16 presents the capture efficiency for viruses (*MS-2* and *Echovirus*). These set of experiments were performed at 2 mL/hr using potential drops of 1.0 V and 1.25 V. The cells collected at device outlets were quantified using plating.

Table 16: Capture efficiency of viruses from recycled water at 1.0 V and 1.25 V potential drop and at 2 mL/hr. (E = 6.7 V/mm, Inlet concentration of cells ~ 10^6 PFU/ml).

Time	***MS-2 (1.0 V)*** 2 ml/hr Plating	***MS-2 (1.25 V)*** 2 ml/hr Plating	***Echovirus (1.25 V)*** 2 ml/hr Plating
t = 15 mins	93.9 ±3.9	92.7 ± 5.2	77.22
t = 30 mins	91.1 ± 1.1	97.6	71.57
t = 45 mins	97.5 ± 0.1	98.9 ± 1.0	77.24
t = 60 mins	88.6 ± 9.9	95.84	74.32

It can be seen from Table 16 that *MS-2* cells were captured with 90-99% efficiency and the capture efficiency drops to around 88% after 1 hour when 1.0 V is applied, whereas the efficiency is consistent at all times at 1.25 V. In the case of the *Echovirus 11*, the capture efficiencies were around 70-80% at all times. Since the viruses are too small to be viewed under a microscope, fluorescent microscopy observations for virus killing under electric fields could not be performed.

Figure 10 shows the effect of pH on the time averaged capture efficiency for Salmonella cells, using 1.0 V potential drop at 2 mL/hr flow rate.

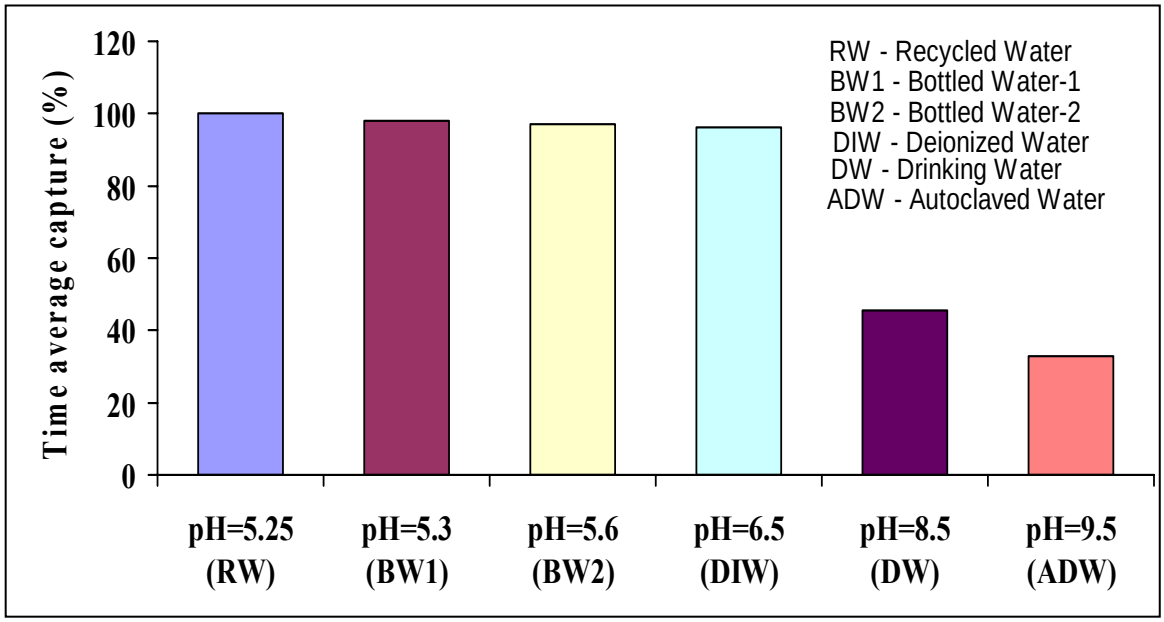

Figure 10: Effect of pH on time averaged capture in microfluidic device.

The capture efficiencies presented in Tables 11-16 show that the capture efficiency is constant over the times sampled. Hence, in Figure 10, the time averaged capture efficiencies are presented for different types of water with varying pH. It can be seen from this Figure that at basic pH values (> pH 7.0), the capture efficiencies are very small, compared to capture efficiencies at more acidic pH conditions (5.25<pH<6.5). This is attributed to the fact that at higher pH values, the gold electrode has an inherent negative zeta potential, and hence the applied positive potential on this electrode has to overcome this inherent negative charge to enable capture. Since the electrostatic

interactions at higher pH values are less attractive compared to the electrostatic interactions at lower pH values (below isoelectric point of gold electrode), the capture is much lower at higher pH values. This follows the same trend as shown in literature by other researchers. Borchardt et al. [90] have shown that the recovery of bacterial cells and viruses from tap water using glass wool fibers decreases at higher pH values, since at this limit, the fiber reaches its isoelectric point, and is no longer electropositive. Hou et al. [11] have also shown that *MS-2* recoveries from Houston tap water decreases with increasing pH values using charge modified microfilters, which is also attributed to the isoelectric point of the filters being reached at higher pH values.

CELL CONCENTRATION FACTOR

To emphasize the importance and scientific relevance of the capture efficiencies given in Tables 11 to 16, we performed a cell conservation analysis in the microfluidic channel. Since the device was fed with cells at a constant volumetric flow rate ($\dot{Q}$ in mL/hr), continuous cell accumulation takes place in the device. If we assume the inlet and exit concentration of cells as θ_{In} and θ_{Cap} (in CFU/mL), respectively, the cell accumulation rate in the channel becomes $(\theta_{In} - \theta_{Cap}) \times \dot{Q}$ (in CFU/hr). Using wetted volume of the microfluidic device, $\forall = W \times L \times h$, the cell accumulation rate ($d\theta/dt$) can be written (in CFU/ml hr), as

$$\frac{d\theta}{dt} = \frac{(\theta_{IN} - \theta_{CAP}) \times \dot{Q}}{\forall} \tag{15}$$

In order to define a cell concentration factor (*CF*) for a desired time period *T*, equation (15) must be integrated in time, and normalized using the inlet cell concentration value (θ_{In}). Assuming approximately constant cell accumulation rates ($d\theta/dt$), as evidenced by constant capture efficiencies shown in Tables 11-16, the concentration factor achieved at the end of time period *T* (in hours) can be calculated as

$$CF = \frac{\theta_{IN} - \theta_{CAP}}{\theta_{IN}} \times \frac{\dot{Q} \times T}{\forall}. \tag{16}$$

The above analysis was based on the cell numbers at the inlet of the device (θ_{IN}). However, the capture results shown in Tables 11-16 were based on the cell numbers in the negative control experiments (θ_{NC}). Due to the tubing and other components of the device, $\theta_{In} > \theta_{NC}$, and due to cell capture $\theta_{NC} > \theta_{Cap}$. Recognizing similarities between the $(\theta_{In} - \theta_{Cap})/\theta_{In}$ term in equation (16) and capture efficiencies defined in equations (13) and (14), we consistently observe $(\theta_{In} - \theta_{Cap})/\theta_{In} > \eta$. Therefore, we can substitute η instead of the $(\theta_{In} - \theta_{Cap})/\theta_{In}$ term in equation (16), as a *conservative estimate* of the concentration factor. This results in

$$CF = \frac{\eta \times \dot{Q} \times T}{\forall}. \tag{17}$$

Using Table 15, the concentration factors achieved within one hour for *Salmonella* cells at 1.0 V, using the wetted volume of the device ($\forall$=0.36 mL) can be obtained. Since the plating based capture efficiency (η_{Plate}) slightly varies by time, we utilized *time-averaged* capture efficiencies of 90.6%, 93.5%, 85.2%, at 2, 4 and 6 mL/hr flow rates. This results in *CF* values of 5, 10.4, and 14.2, for 2, 4 and 6 mL/hr flow rates,

respectively. Therefore, assuming uniform cell distribution in water and constant capture efficiency, the pathogen concentration in the device increases by *CF* folds for a given time period *T*. The sample volume reduction (*SVR*) achieved by the device can be calculated as

$$SVR = \frac{\dot{Q} \times T}{\forall}. \tag{18}$$

Within an hour *SVR* values of 5.55, 11.11, and 16.67 are observed at 2, 4 and 6 mL/hr flow rates, respectively. Comparing equations (12) and (13),

$$CF = \eta \times SVR. \tag{19}$$

We must note that both the *CF* and *SVR* values increase linearly with time and the flow rate, and reduction in the wetted volume $\forall$ is crucial for enhanced results. However, the capture efficiency (η_{Plate}) and its stability with time remains the most crucial issue in device performance.

Based on the capture efficiency results presented in Tables 11 – 16, 90 to 99% of *E. coli, Salmonella, Pseudomonas* and *MS-2* are captured in the device. Capture efficiency for *Echovirus* is about 75%. Consistency of the capture efficiency for most pathogen types makes this device nonspecific to the pathogen type. This is usually not the case for filtration based concentration methods, where filter pore size is optimized for specific organisms. In addition, capturing viruses using ultrafiltration and nanofiltration systems can be rather expensive and laborious. However, the microfluidic device captures viruses based on their surface charges and delivers consistently high capture efficiencies, without the need for any chemical additives.

Capture efficiencies reported in the literature mostly utilize the inlet concentration as a reference. All capture efficiency calculations presented in this study are based on the negative control data. This is a major difference between this paper and other concentration based studies reported in the literature (Tables 1 and 2). Our approach, based on the negative control experiments, accounts for microorganisms that may have adhered to tubing and other accessories that are part of the capture system. If the inlet samples were used as the reference for efficiency calculation instead of the negative control, number of the captured cells would increase by half to one log, and this would increase the overall capture efficiency of the device.

To our knowledge, this is the first study using real-time PCR to validate the device capture efficiencies obtained by plating methods. Previous studies, summarized in Tables 1 and 2, were based on plating. Hence, those studies did not presumably account for the dead, and viable but unculturable cells, which may arise as a result of the cell capture method.

FULL-SCALE PRESSURE DROP AND PUMPING POWER COMPARISONS

Development of a continuous, species non-specific pathogen capture and concentration system from large volumes of water is one of the primary motivations of this study. The prototype device with 0.36 mL wetted volume can efficiently capture pathogens at 6 mL/hr flow rate. We have chosen continuous sampling of water at 5 L/hr as a target for terrestrial and space applications. We plan to address the drastic differences between the single channel and target flow rates by stacking multiple identical channels in planar arrays. For example, using our current design, we can match

the 5 L/hr target flow rate using 2500, 1250 and 835 microchannels at 2, 4 and 6 mL/hr, respectively. With the advent of micro fabrication technologies, it is possible and affordable to fabricate arrays made out of several thousand identical microchannels [91]. An important requirement in device design is the final sample volume, which needs to be compatible with the existing detection methodologies.

The electrical power required to capture pathogens, and the pumping power required to maintain 5 L/hr flow rate are critical parameters that need to be considered. In Table 17, we present the power requirements and the final concentrated volume for using 2500, 1250 and 835 identical microchannels, operating at 2, 4 and 6 mL/hr, respectively.

Table 17: Device parameters to sample water at 5 L/hr at various conditions.

	2 mL/hr	**4 mL/hr**	**6 mL/hr**
Total number of channels required	2500	1250	835
Full scale pumping power	4.1 μW	8.3 μW	12.4 μW
Full scale electrical power	50 mW at 1.0 V 80 mW at 1.25 V	25 mW at 1.0 V 40 mW at 1.25 V	17 mW at 1.0 V 26.8 mW at 1.25 V
Total concentrated volume	900 ml	450 ml	300 ml
Concentration factor at 90% efficiency	5	10	15

The total electrical power (P_E) is obtained from the current (I) and voltage (V) characteristics of the single channel device (Table 10), using $P_E=nVI$, where n is the total number of channels required to maintain 5 L/hr flow rate. The total pumping power (P_{pump}) is obtained using the flowrate and pressure drop of a single channel, and using $P_{pump} = n\dot{Q}\Delta p$ (Table 10). At 6 mL/hr, the total number of channels required to sample at 5 L/hr is 835, and the total power required to pump the fluid is on the order of 0.012 m*W*. This is four or five orders of magnitudes smaller than the power required for ultrafiltration (~0.2-0.3 *W*) [15] and nanofiltration (~5-10 *W*) [92] systems at the same flow rate. The electric power is on the order of 30 mW. These power estimates neglect power losses in various components and the pressure drop in tubing. Therefore, with a *conservative estimate*, we envision the total power requirement of the pathogen capture and concentration system to be on the order of 0.1 W. Using 835 channels operating at 6 mL/hr, the device samples 5 L of water within an hour and captures 90~99% of the pathogens in a total wetted volume of 300 ml. Therefore sample volume reduction (*SVR*) of 16.67 can be achieved within an hour. With at least 90% capture efficiency the device should yield a concentration factor (*CF*) of 15.

IN-SITU ANALYSIS OF ADHESION ON MICROFABRICATED GOLD ELECTRODES

INTRODUCTION

When bacterial cells are in close proximity to a solid surface (<100 nm from surface), various interaction processes including van der Waals interactions, hydrophobic interactions and electrostatic interactions play a vital role in determining the adhesion process. However, electrophoretic transport and electrostatic interactions between charged surfaces play a vital role in situations where the bacterial cells need to get closer to a solid surface from the bulk flow region, so that other interactions and adhesion can occur. In order to gain a better understanding of bacterial attachment to charged substrates in flow based systems, systematic studies of capture and immobilization of bacterial cells on a surface is essential.

In the past, many researchers have used flow based systems to study bacterial adhesion to surfaces in micro-scale devices by applying external voltages. These include parallel plate and stagnation point flow chambers, rotating disk systems and cylindrical channels [93-98]. Design of such systems requires careful consideration of the time scales involved in fluid and particle motion. These systems often neglect various electrochemistry effects that arise due to the presence of electric fields. Quantification of adhesion in these systems was primarily based on microscopy, which requires an efficient particle tracking algorithm [99]. In-situ quantification methods are often more reliable than indirect methods that involve removing the substrate from the flow

chamber following capture, washing off cells that did not adhere to the electrode, and counting the captured cells under a microscope. One of the main advantages of in-situ microscopy analysis is that adhesion and desorption characteristics of bacterial cells can be studied as a function of flow parameters in detail.

In this section, in-situ quantification of microbial capture was studied by applying pressure driven flow in a parallel plate microfluidic chamber with an external potential difference. The objective of this study was to analyze the effect of electric field and applied flow rate on cell capture using image analysis by particle tracking. The effect of flow on capture was delineated by studying the capture trends at different locations on the electrode surface with respect to flow velocity and wall shear stress contours generated from CFD simulations. During the capture experiments, electric currents due to Faradaic processes were also monitored to predict the apparent electric field in the bulk fluid that is responsible for electrophoresis of bacterial cells in the system.

BACTERIAL STRAIN AND MEDIA

Salmonella Newport, with an inlet concentration of ~ 10^6 *CFU/mL* (*CFU*: Colony forming units) was utilized for the capture experiments. The cells were initially grown at 37ºC in unamended Luria-Bertani (LB) broth. Following this, the cells were centrifuged (3300 × *g)* and washed three times using 10 *mL* of filter sterilized water. The washed cells were then resuspended in 40 *mL* of fresh buffer for experimentation. The cells were quantified by plate counts and the inlet concentration of cells was between 3.0×10^6 and 5.0×10^6 *CFU/mL* during every experiment. The cells were tested in the

microfluidic device within 4-6 hours of preparation. Potassium phosphate buffer, with a pH of 5.5 and ionic strength of 1 *mM* was used as the suspending medium. The cells were tagged with *Bac*Light™ Bacterial Viability Kits (Invitrogen) during culturing, which enables them to fluoresce when illuminated with UV light of appropriate wavelength.

MICROFLUIDIC DEVICE FABRICATION

The microfluidic device used for the capture studies was fabricated using standard photolithography techniques. The electrodes were patterned on a 75 × 50 *mm* glass slide. Prior to patterning, holes were drilled on the slide (anode only), for inlet and outlet tubing connections (Figure 11a). Following this, positive photoresist (SC1805) was patterned on the slide using an appropriate UV mask (1 μm thickness) using spin coating, followed by exposure to UV light with a mask aligner. After development, a glass slide with the photoresist pattern (as shown in Figure 11b) was produced. This photoresist patterned slide was then exposed to a plasma etcher for 10 seconds, to remove any additional layer of photoresist that was not removed during the development process. Finally, a 5 nm layer of chromium, followed by a 15 nm layer of gold was deposited on the patterned slide. Rinsing the patterned slide with acetone in a sonicator removes the photoresist. Patterned gold electrodes that were used as the microchannel walls are schematically shown in Figure 11c. Both the top and bottom electrodes were patterned using the same procedure. Gold was used as the electrode material since it has an oxidation potential higher than the potentials used in this study (1.0 *V* and 1.25 *V*). In addition, gold is a noble metal and it is biocompatible.

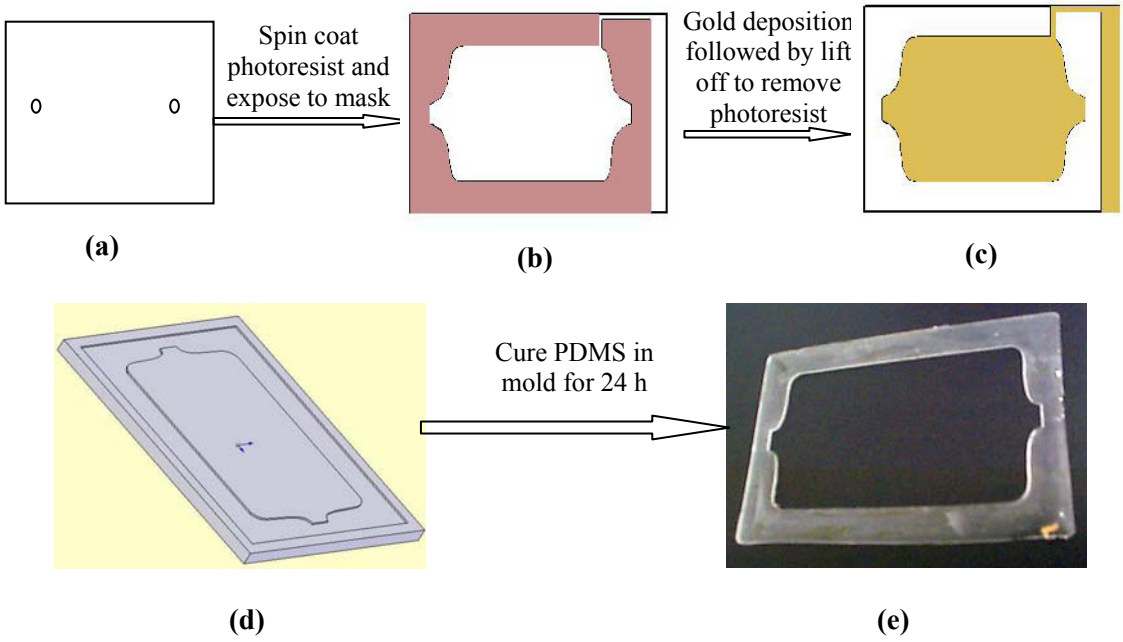

Figure 11: Schematics of device fabrication (a) Plain glass slide with holes, (b) Photoresist patterned glass slide, (c) Gold patterned electrode, (d) CNC mold from plexiglass, (e) PDMS spacer after peel off.

The spacing between electrodes was created using a PDMS spacer. The spacer was fabricated by curing equal parts of PDMS resin and curing agent in a CNC machined plexiglass mold of desired shape for 24 hours, followed by peeling off the dried PDMS (Figures 11d and 11e). The shape of the channel ensures that flow in the channel develops gradually. Both the PDMS spacer and patterned gold electrodes were

exposed to plasma oxygen gas in a plasma etcher. This activates functional chemical groups on the surface of the spacer and electrode. Following this, the spacer was sandwiched between the electrodes and the system was kept under clamps for 30 minutes to ensure good sealing. Figure 12 shows the assembled microfluidic device that was used for microscopy experiments. Two different channel heights (150 and 450 μm) were tested in this study creating external electric fields of 2.78 and 8.34 *V/mm*, respectively. The length (L) and width (W) of the channel were 62.30 and 35.60 *mm*, respectively.

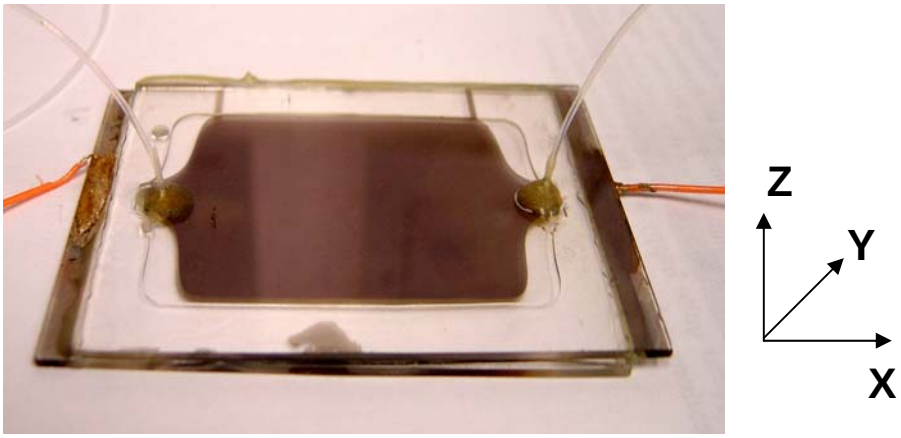

Figure 12: Assembled microfluidic device.

MICROFLUIDIC DEVICE DESIGN AND PRINCIPLE OF OPERATION

Pressure driven flow is applied through the channel to maintain the flow, while a constant potential difference between the electrodes creates a uniform electric field (E). The assumption of uniform electric field is a simplification, which neglects the effects of ion distribution and Faradaic reactions at the electrode-electrolyte interfaces. Using the simplified model, the constant electrophoretic velocity (V_{EP}) with which negatively charged particles travel towards the anode can be represented as

$$V_{EP} = \mu_{EP} E\,, \tag{20}$$

where μ_{EP} is the electrophoretic mobility of microorganisms. We reported electrophoretic mobility and zeta potential measurements of different bacterial cells suspended in water in Tables 5 and 6. We utilized the smallest electrophoretic mobility (-0.31 μm-cm/V-sec) in this study for the microchannel design. This ensures that even the slowest moving microorganisms are captured before they leave the channel.

Two time scales of particle motion are essential for device design. These include the time required for particle migration towards the anode (t_M), which can be predicted as

$$t_M = \frac{h}{V_{EP}}, \tag{21}$$

and the particle residence time (t_R) in the channel, which can be predicted as

$$t_R = \frac{L}{V_{AVE}}, \tag{22}$$

where h is the height of the channel and V_{AVE} is the channel average fluid velocity. For pressure driven flows, the maximum flow velocity happens in the middle of the channel, and its magnitude is 1.5 V_{AVE}. Therefore, $t_M/t_R << 1$ is a critical design constraint in selection of the channel dimensions and the flow rate. Electric field experienced by particles in the bulk fluid is the critical parameter that dictates particle motion towards the anode. As stated earlier, the assumption of uniform electric field is invalid in real systems. At high applied potentials, charge separation due to ion redistribution and electrochemical reactions due to Faradaic processes influence the bulk electric field experienced by the particles in solution in a non-trivial way. Predicting the apparent electric field in the bulk fluid is critical to calculate the time scales for particle migration accurately based on equations (20) and (21). This could be done by monitoring electric currents in the device as a function of time. In the following section, we present current measurements performed in the microfluidic channel, at no flow, and two different volumetric flow rate conditions (2 and 6 *mL/hr*) under an applied potential difference of 1.25 *V*. Based on these measurements, the apparent electric field in the bulk solution, and hence, the time scales for particle motion were calculated.

APPARENT ELECTRIC FIELD IN MICROCHANNEL

Steady electrokinetic flows in microfluidic devices require sustaining steady electric current in the system. For small applied potentials (≤ 25 *mV*), electrochemical reactions at the electrode-electrolyte interfaces can be neglected. Under such conditions, electrodes are considered to be ideally blocking (or ideally polarizable). In such a system, when an external potential difference is applied across the two electrodes, the electric

double layers (EDL) at the electrode-electrolyte interfaces get charged. This is a non-Faradaic process, which results in charge separation of the ionic species, setting up a counter electric field *(E_C)* opposing the external field *(E)*. The apparent electric field ($E_{APP}=E - E_C$) experienced by the charged species is the critical parameter that dictates particle electrophoresis towards anode, and sets up a non-Faradaic current in absence of electrochemical reactions. After a certain time, the counter field eventually balances the external field. There will be no electrophoresis in the system beyond this time scale. Dynamics of this idealized behavior was described by Bazant et al. [100].

In microfluidic systems with electrokinetic actuation, applied potentials are usually much larger than 25 *mV*. Since we utilized potential differences of 1.0 and 1.25 *V* in our study, the idealized behavior explained above breaks down. At these potentials, steady electrokinetic flow is maintained by *electrochemical reactions* that occur on electrode surfaces, which sustains the current and electric field despite the charge separation. The resulting electric field will depend on the electrochemistry and applied potential in a non-trivial way. These types of processes are termed as Faradaic processes, which are associated with electron transfer across the interface leading to reduction or oxidation of species present at the interface. The Faradaic currents due to these processes are proportional to the overall reaction rate, which must be determined experimentally.

In this section, we present current measurements in the microchannel, based on which the apparent electric field in the bulk solution and hence, the particle migration time scales were estimated.

Current Measurements

In a non flowing system, Faradaic reactions would establish bulk concentration gradients over a long time scale. However, convective effects will eliminate these transients and stabilize the electric current due to continuous supply of fresh buffer solution and washing out of the reaction products at a constant rate [101]. This is demonstrated in Figure 13, where we present time variation of electric current in the microfluidic channel (L=62.30 mm, W=35.60 mm, h=150 μm). A 1 mM phosphate buffer at pH=5.5 with and without a pressure driven flow was utilized, while imposing 1.25 V potential difference between the two electrodes (8.34 V/mm). Variation of current as a function of time is presented at no flow and two different flow rates (0, 2 and 6 mL/hr). Current was monitored using a digital multimeter and measurements were recorded every 15 seconds until a steady state was reached.

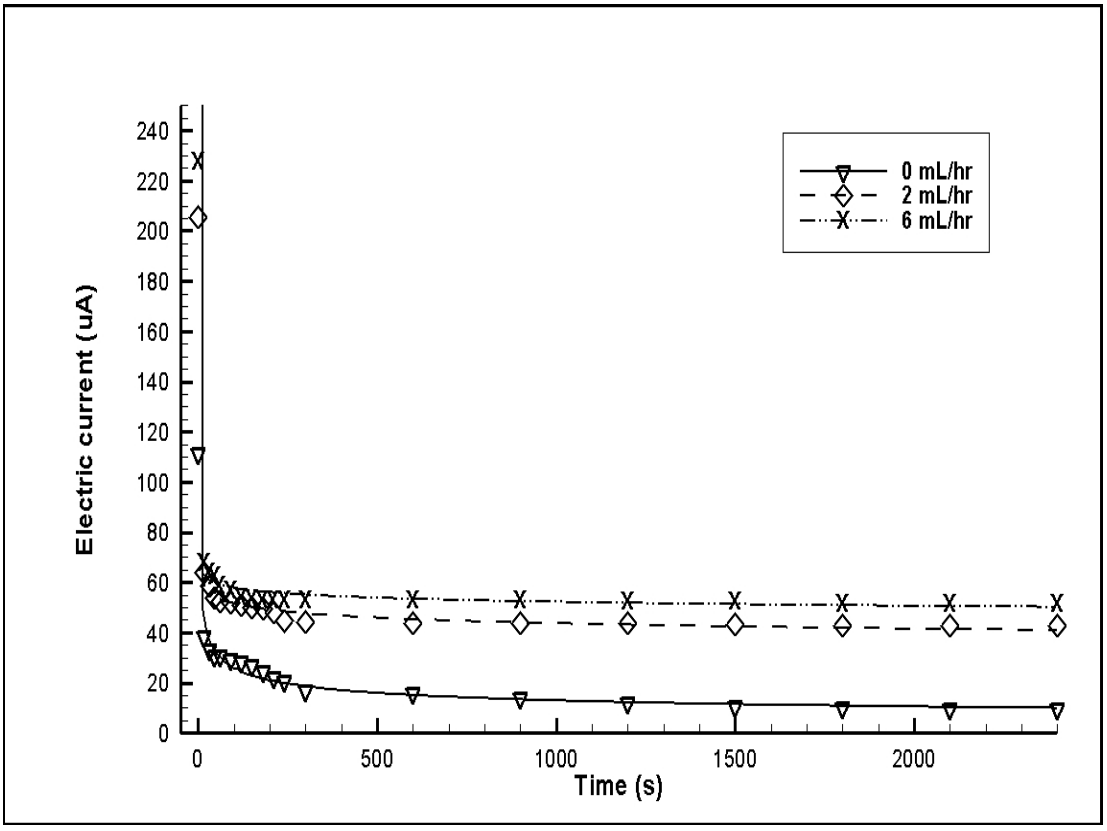

Figure 13: Time variation of electric current of 1 *mM* phosphate buffer solution (pH=5.5) in the microfluidic channel at 8.33 V/mm, under no-flow and various flowrates.

After initial transients experienced by all three cases, the nonflowing system exhibits slow decay in electric current that is induced by gradual build up of bulk concentration gradients. Initially, the system behaves like an ideal capacitor, where the current drops exponentially from its maximum value, with a response time equivalent to the double layer charging time-scale. The response time for such systems has been

predicted to be on the order of $\lambda_D L/D$ [100], where λ_D is the EDL thickness, L is the electrode separation and D is the diffusivity of the ions in the buffer. For our experiments, typical values of λ_D, L and D are 10 *nm*, 150 μm and 10^{-5} cm^2/sec respectively. This results in a response time of the order of milliseconds. At the range of potentials applied in this study, the electrodes do not behave as ideally polarizable or ideally blocking electrodes. Electrochemical reactions occur at the electrode-electrolyte interface, giving rise to charge transfer reactions (oxidation at cathode and reduction at anode). These charge transfer reactions enable us to sustain a Faradaic current in the system. Hence, the current in our system reaches a steady value and then drops at a very slow rate after the initial capacitive charging.

With flow in the system, the current follows the initial capacitive charging transient behavior. After this however, the current has a finite value (~45 and 55 μA for 2 and 6 *mL/hr*) and it remains steady at this value for a long time (hours). We attribute this behavior to the convective effects due to the external pressure driven flow. Flow maintains a constant supply of ions in the system which enables the device to overcome charge separation, and it still maintains a steady electric current that is responsible for electrophoretic transport of charged species in the device. The external flow induces concentration boundary layers due to polarization along the electrode-electrolyte interface in the channel. Hence, delineating the apparent electric field in the channel requires detailed local information on ion concentrations, which vary with position.

FLOW MODELING

Modeling of fluid flow in the channel is essential to predict the different time scales involved in fluid and species transport in the channel due to external flow. Based on the microchannel design, the inlet and outlet were at the top of the channel (Figure 12). Hence, the pressure driven flow results in injection of fluid at the inlet and suction of the same fluid at the outlet of the channel, resulting in Hele-Shaw type flow patterns [102]. This type of flow is two-dimensional with X and Y components of the velocity varying parabolically in the Z direction. Flow field simulations were performed using a commercial CFD code (Fluent) with second order spatial accuracy to predict the velocity and streamline patterns in the channel. Steady state Navier Stokes equations were solved subject to no-slip boundary conditions on the walls. A tetrahedral unstructured mesh, with 95,000 elements was generated using the Gambit software [103].

Figures 14a, 14b and 14c present normalized streamwise velocity contours at various Y-Z, X-Z and X-Y planes, respectively with an inlet flow rate of 6 *mL/hr* and 150 μm spacing between the electrodes. The X, Y and Z axes were non-dimensionalized using the height of the channel (150 μm). The velocity was non-dimensionalized using the average velocity near the inlet of the channel (74.13 $\mu m/second$).

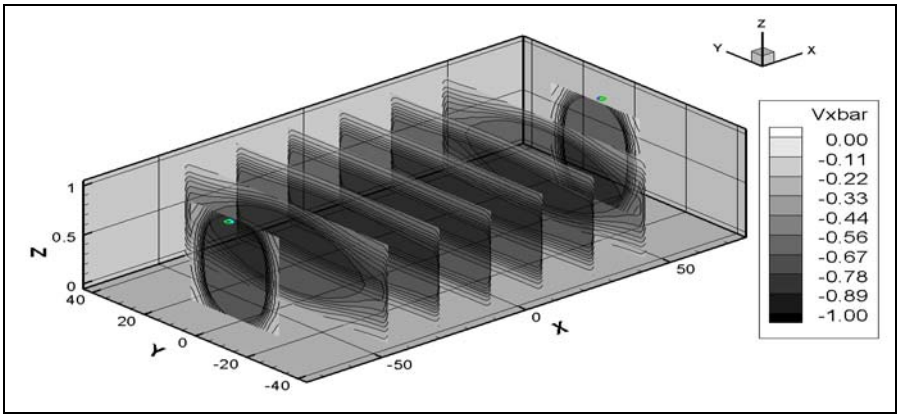

(a)

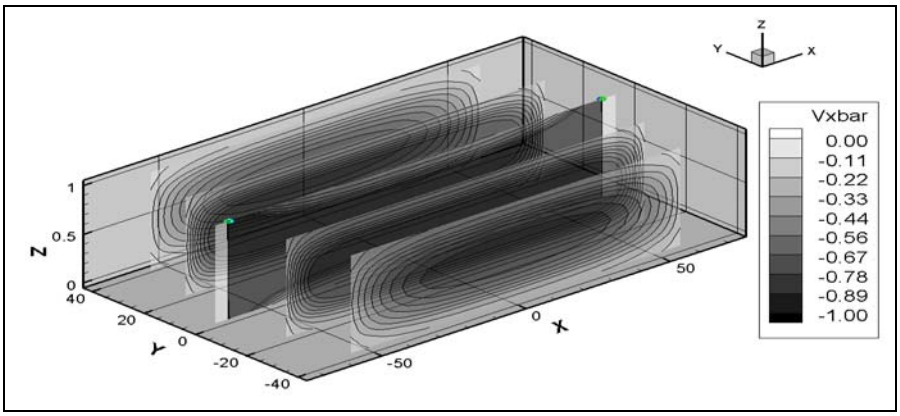

(b)

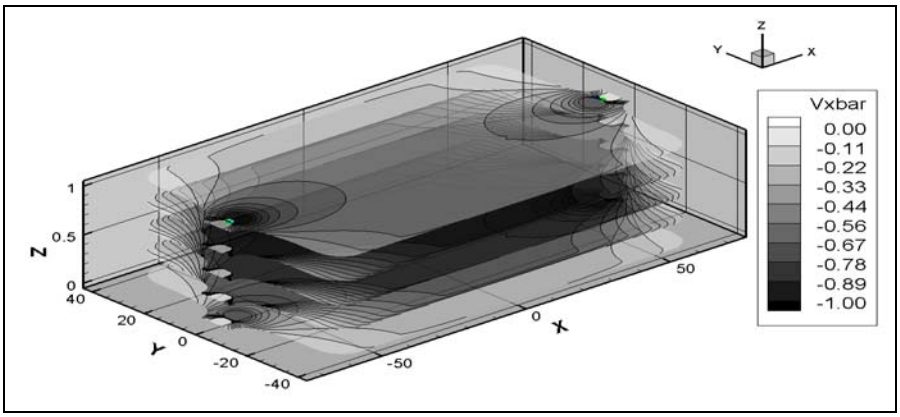

(c)

Figure 14: Numerical results of normalized streamwise velocity contours at various (a) X-Z, (b) Y-Z and (c) X-Y planes. Length scales are normalized using h=150 μm and the velocity is normalized using the inlet velocity=74.13 $\mu m/s$.

Figures 14a and 14b show that the velocity profile is symmetric about the *Y*-*Z* and *X*-*Z* planes at the center of the channel. Based on Figure 5c, it can be seen that the *X*-component of the velocity is independent of the *X* and *Y* coordinates of the channel. Hence the flow in the channel is fully developed and the fluid has a parabolic velocity profile along the *Z* direction, with maximum velocity at the center of the channel, as predicted by Hele-Shaw flow equations [102]. *Y*-component of the velocity shows similar trends (data not included). Figure 15 presents the streamline patterns at center plane of the channel. Based on this figure, it can be seen that the flow in the channel is two dimensional.

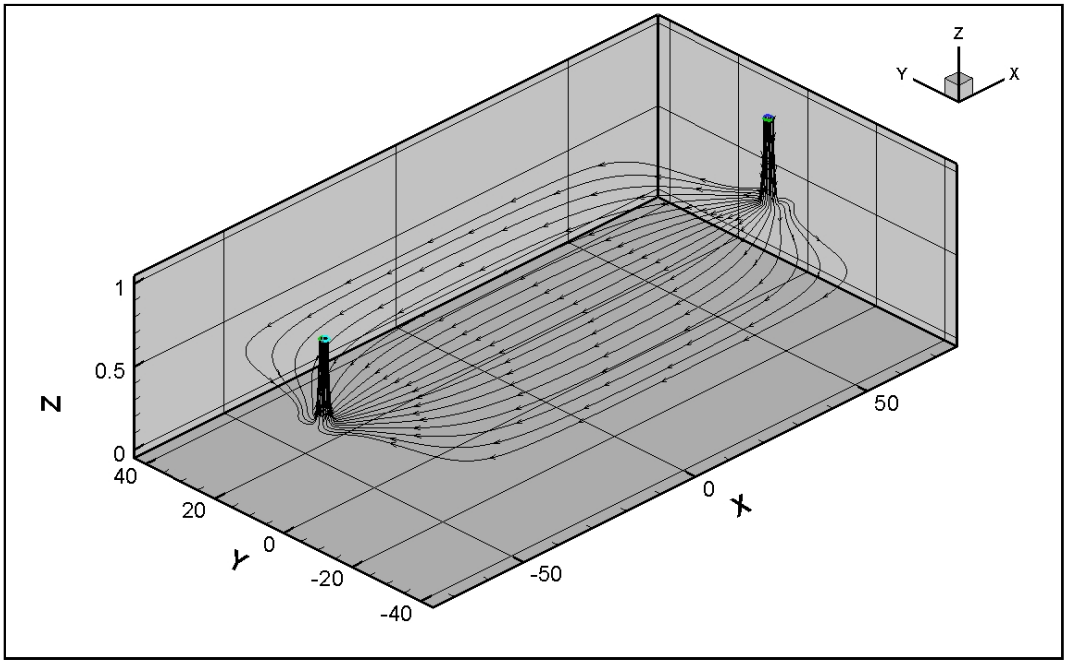

Figure 15: Numerically predicted streamline patterns along the center of the channel.

Figure 16 presents the shear stress contours on the channel top wall (in mN/m^2). Wall shear stress is important to quantify the amount of shear force acting on bacterial cells attached to the anode. Since shear force is responsible for the release of captured cells, it is critical to analyze capture at different locations on the electrode surface as a function of shear stress at these locations.

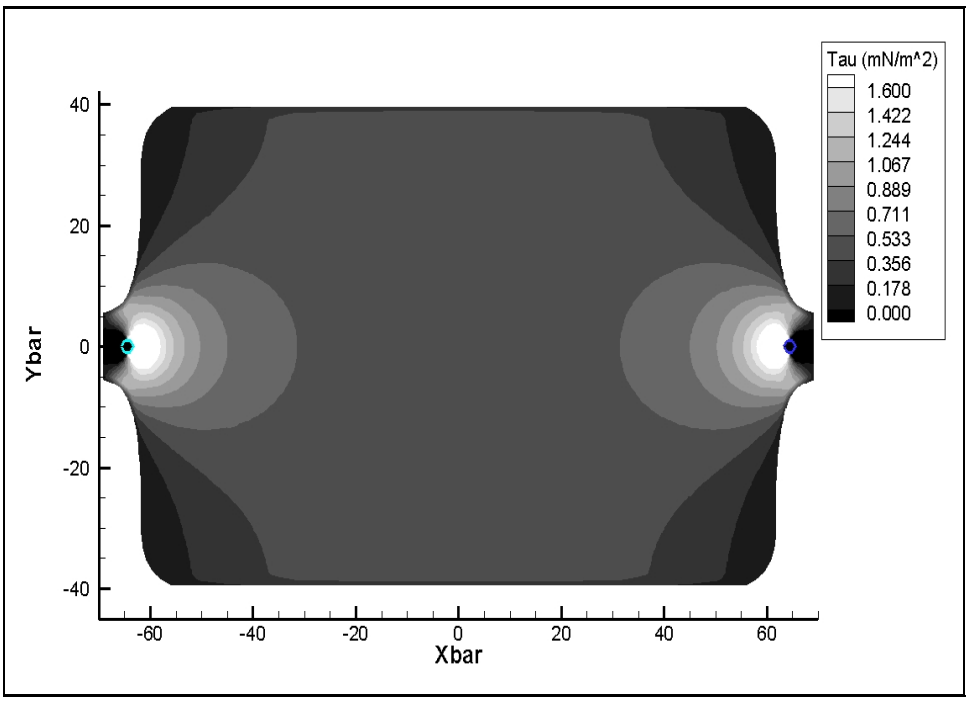

Figure 16: Numerically predicted shear stress contours on the anode.

Based on Figure 16, 20 different locations on the electrode surface with various shear stress values were identified. Capture at these locations was analyzed by sampling images at the top electrode surface at each location as a function of time, followed by image processing. In the next section, we describe the procedure utilized for particle tracking and image processing to analyze capture as a function of time.

EXPERIMENTAL SETUP AND DATA ANALYSIS

The assembled microfluidic device shown in Figure 12 was imaged using an Olympus BX61 epifluorescence microscope. Using an external power supply, a potential difference was applied between the two electrodes, with the top electrode surface having a positive charge and the bottom electrode having a negative charge. Since the bacterial cells have a net negative surface charge, capture occurs on the top plate. The specific gravity of the bacterial cell used in this study was greater than 1. This ensures that capture occurring on the top plate overcomes the gravitational effects. A syringe pump was utilized to pump bacterial cells suspended in phosphate buffer (1 *mM*, pH=5.5) into the device at constant flow rates of 2 and 6 *mL/hr*. Two different channel heights (150 and 450 μm) were tested in this study creating external electric fields of 2.78 and 8.34 *V/mm*, respectively. Each set of experiments were repeated three times to ensure repeatability of experiments and data quality. Based on Figure 16, 20 different locations on the electrode surface with various shear stress values were identified. Capture at these locations was analyzed sequentially by sampling images at every location as a function of time. Figure 17 shows a schematic of the locations at which images were taken.

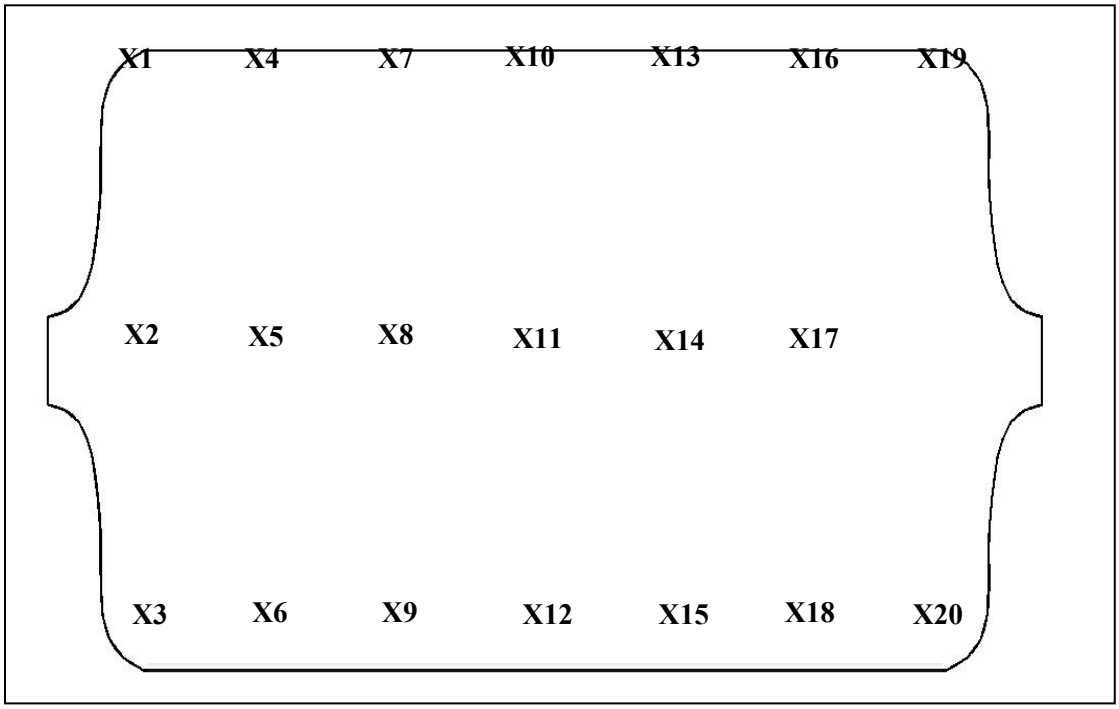

Figure 17: Image sampling locations on the anode.

Imaging Procedure and Image Processing

Images were collected using a 10X objective focused on the top electrode. The field of view based on the objective magnification was 660×660 μm (1024×1024 pixels). Images were sampled at every location shown in Figure 8 sequentially, starting from location number 1. Two images were collected within 10 seconds of each other at every location, before moving to the next. This is a necessity due to the large surface area of the anode, and the magnification requirements utilized to observe bacterial cells. The

captured cells were identified by comparing the centroid location of each cell between the two images. This procedure was repeated every 10 minutes during the course of the experiment for one hour. Sequentially sweeping 20 different locations shown in Figure 17 require approximately 380 seconds, inducing time variance in the capture data that will be presented in the next section.

The images were processed using Image-J software [104]. Successive snapshots that were within 10 seconds of each other were analyzed to compare the centroid location of each cell between the two successive images. The average size of Salmonella cells were reported in Table 9 as 1.9 μm (2.94 pixels). The bacterial cells were assumed to be captured, if the centroid movement between successive images was less than two bacterial lengths (~6 pixels). This is a reasonable assumption since the cells move past the field of view with an average velocity of approximately 200 pixels/s at 6 *mL/hr* flow rate.

Protocol for Plating Quantification

Three different dilutions of each sample collected from the outlet of the microfluidic device were prepared in phosphate buffer. Ten (10 μL) of sample mixed with 90 μL of phosphate buffer were plated on Luria-Bertani (LB) agar and incubated for 16-18 hrs at 37 ºC prior to enumeration. The colonies were counted and averaged to quantify the concentration of cells in the original sample and results were expressed as CFU/mL.

RESULTS OF CAPTURE EXPERIMENTS

Figure 18 shows snapshots of the top electrode surface, after flowing *Salmonella* cells for one hour at a flow rate of 6 *mL/hr*, without (a) and with (b) applying an electric field, respectively.

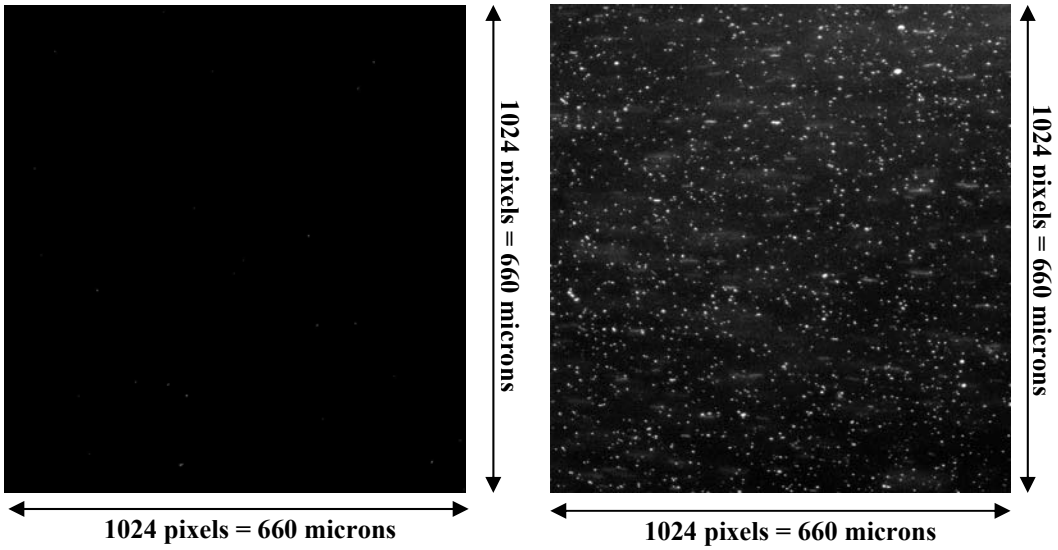

Figure 18: Bacterial cell distribution on the anode without (a) and with (b) and externally applied electric field of 8.34 *V/mm* at 6 *mL/hr* flowrate obtained within an hour of operation.

Without an electric field, the bacterial cells do not experience any electrophoretic motion. Hence, as evidenced in Figure 18a, there is no cell capture on the anode since the cell-surface interaction forces are not strong enough to overcome the wall shear stress due to external flow. Without an externally applied positive charge, both the gold electrode and bacterial surface have inherent negative zeta potential, resulting in repulsive electrostatic cell-surface interactions. This prevents immobilization of cells on the anode. However, when an external potential difference is applied in the channel, significant capture is seen on the anode. In Figure 18b uncaptured cells that flow past the field of view are observed as large streaks.

Figure 19 presents the number of captured cells per field of view ($660 \times 660\ \mu m$) at various locations sampled on the electrode surface as a function of time at 6 *mL/hr* flow rate and 1.25 *V* potential drop. Each location is labeled using a different color/symbol combination to differentiate the capture trends at various locations.

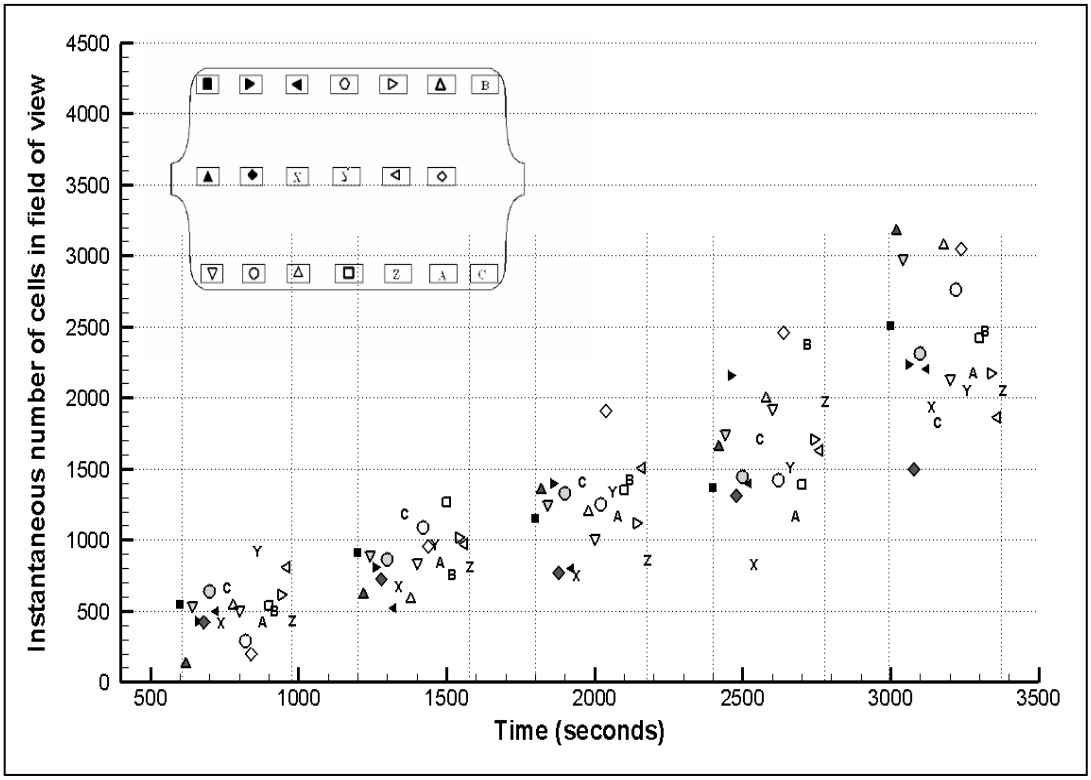

Figure 19: Number of captured cells per interrogation area, sequentially obtained at 20 different locations on the device at 6 *mL/hr* flow rate and 8.34 *V/mm* electric field.

Sequential sweeping of every location results in time variance in capture data. Bacterial capture varies on the electrode based on the shear stress at a particular location. Even though the velocity contours presented in Figure 14 show symmetry in flow patterns about the center of the channel, capture trends at symmetric locations do not

show similarities at every location. Immobilization of cells and hence capture is dependent on various cell-surface interaction forces. Of these interactions, van der Waals and electrostatic interaction forces do not change with location on the electrode surface. However, the hydrophobic and steric interaction forces depend on wettability and surface roughness, which may vary at different locations on the electrode [105]. In addition to cell movement due to pressure driven flow in the channel, presence of flagella in *Salmonella* Newport causes differential cell motility at different locations in the channel. Hence, variable capture trends are observed at different locations on the electrode.

Capture data presented in Figure 19 was averaged over all imaged locations to obtain an estimate of mean capture on the top electrode surface as a function of time. Figure 20 presents the average number of cells per field of view captured on the electrode surface as a function of time for two different electric fields (E=2.78 *V/mm* and 8.34 *V/mm*) at 6 *mL/hr* flow rate.

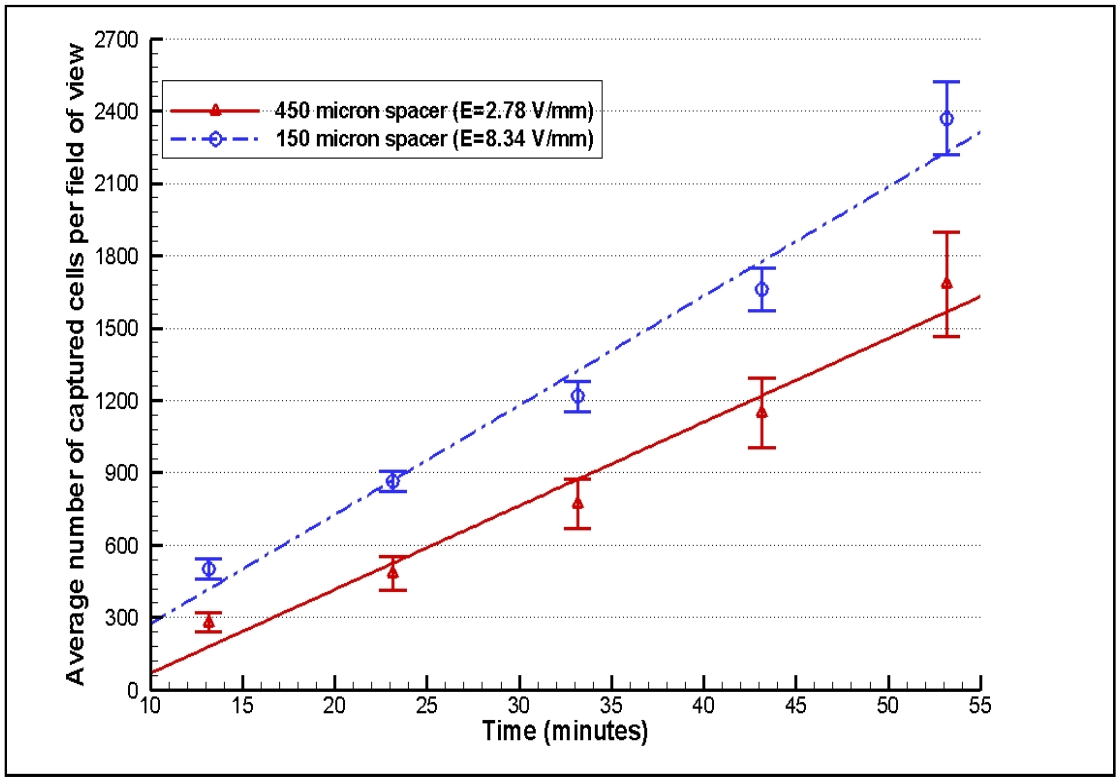

Figure 20: Time dependence of capture (average number of captured cells per field of view) at various electric fields and 6 *mL/hr* flow rate. Each data point has 380 s variation in time, induced by the experimental protocol.

The P values associated with capture data comparisons (based on paired-t tests) between different applied electric fields are presented in Table 18.

Table 18: P-values for comparison of capture data between different experimental treatments (A P value < 0.05 represents significant difference based on paired t-test).

Experimental Treatment	Time of Capture				
	10 mins	20 mins	30 mins	40 mins	50 mins
Electric field variation	0.009*	0.000*	0.001*	0.001*	0.01*
Flow rate variation	0.441	0.701	0.172	0.269	0.267
Shear stress variation at 2.78 V/mm	0.114	0.369	0.254	0.982	0.659
Shear stress variation at 8.34 V/mm	0.126	0.050*	0.268	0.824	0.700

Sequential sweeping through 20 different locations takes 380 seconds, which induces time variance in the abscissa that is omitted from the figure for clarity. The ordinate error bars represent the uncertainty in capture across different locations, which were calculated as the standard error ($SE=\frac{\sigma}{\sqrt{N}}$) of the raw data presented in Figure 19, where σ is the standard deviation of capture and N is the number of locations at which images were sampled. The uncertainty in capture is between 5-10% at all times. It can be seen from this figure that average number of captures cells increases approximately linearly with time for both electric field conditions, and the capture is significantly higher at higher electric fields.

The constant capture rates presented in Figure 20 were validated by performing indirect quantification studies using culture based methods. In a separate experiment, with an external potential difference applied in the channel (1.25 *V*), cells at the outlet of

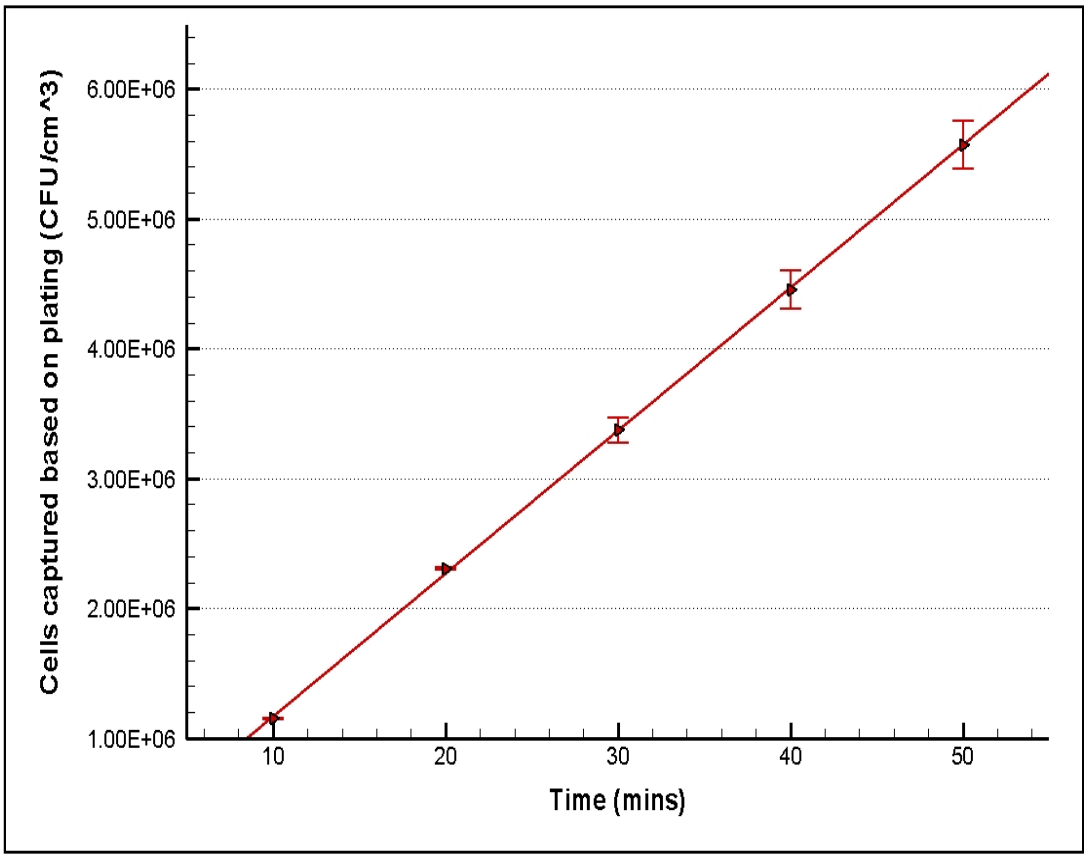

Figure 21: Quantification of capture in the device based on plating at 2 *mL/hr* flow rate and 8.33 *V/mm* potential difference.

the microfluidic device were collected at 2 *mL/hr* external flow rate. Capture in the device was quantified indirectly by comparison of inlet and outlet cell concentrations (*CFU/mL*) based on plating. Figure 21 presents the number of cells captured per unit volume of sample (*CFU/mL*) collected at the device outlet as a function of time based on plating at 2 mL/hr flow rate and 1.25 *V* potential drop.

The error bars in the data correspond to standard error in capture based on three repetitions. It is critical to note that capture based on microscopy was quantified per unit area of the electrode (CFU/cm^2), whereas capture based on plating was quantified per unit volume of the microfluidic device (CFU/cm^3). Hence, the actual values itself cannot be compared. However, it can be seen from Figures 20 and 21 that both microscopy and plating predict linear trends in capture with similar cell accumulation rates.

Figure 22 presents the variation in average number of cells per field of view, captured on the electrode as a function of time at two different external flow rates (2 and 6 *mL/hr*) under a fixed electric field of 2.78 *V/mm*.

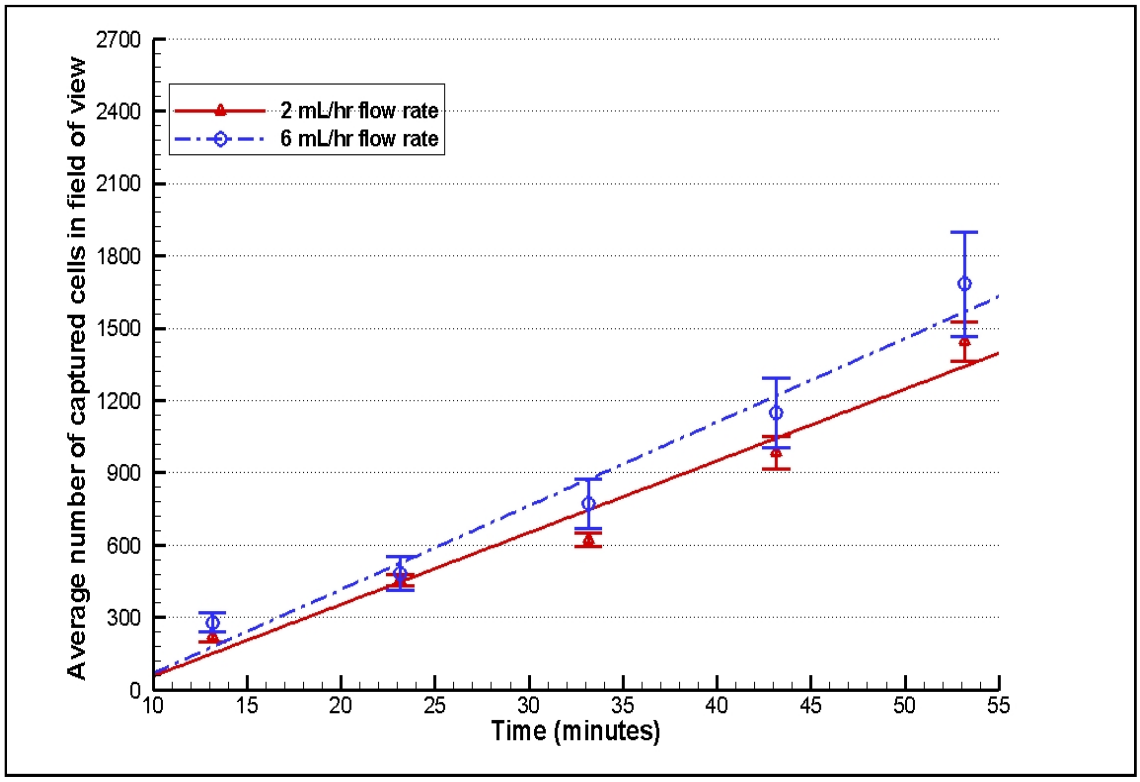

Figure 22: Time dependence of capture at various flowrates and fixed electric field of 2.78 *V/mm*. Each data point has 380 s variation in time, induced by the experimental protocol.

The P values comparing significant differences in capture between different flow rates are shown in Table 18. The ordinate error bars represent uncertainty in capture data across different locations. Figure 22 shows slightly higher capture at 6 *mL/hr* flow rate compared to the capture at 2 *mL/hr* flow rate. Based on the current measurements, it was

shown in Figure 4 that higher flowrates resulted in larger steady electric currents. This may induce slightly larger electrophoresis/electrostatic interactions at higher flowrates, resulting in increased capture.

Bacterial cells experience higher shear force at higher flowrates. This is expected to prevent their adhesion to the electrode surface. Hence, it is critical to quantify capture in the single channel device as a function of shear stress on channel walls. In order to do this, locations with similar shear stress values were picked from Figure 17 and capture at these locations was averaged. Based on Figure 16, locations 1, 3, 4, 6, 16, 18, 19 and 20 were identified as low shear stress areas, with an average shear stress value of 0.62 mN/m^2. Similarly, locations 2, 5, 7, 8, 9, 10, 11, 12, 13, 14, 15 and 17 were identified as high shear stress areas, with an average shear stress value of 1.55 mN/m^2. Figure 23 presents the variation in average capture as a function of time at locations with average shear stress of 0.62 and 1.55 mN/m^2 under 2.78 and 8.34 V/mm electric field. The P values comparing significant differences in capture between different shear stress locations are presented in Table 1. Error bars in the figure represent the uncertainty in capture across different locations with similar shear stress values.

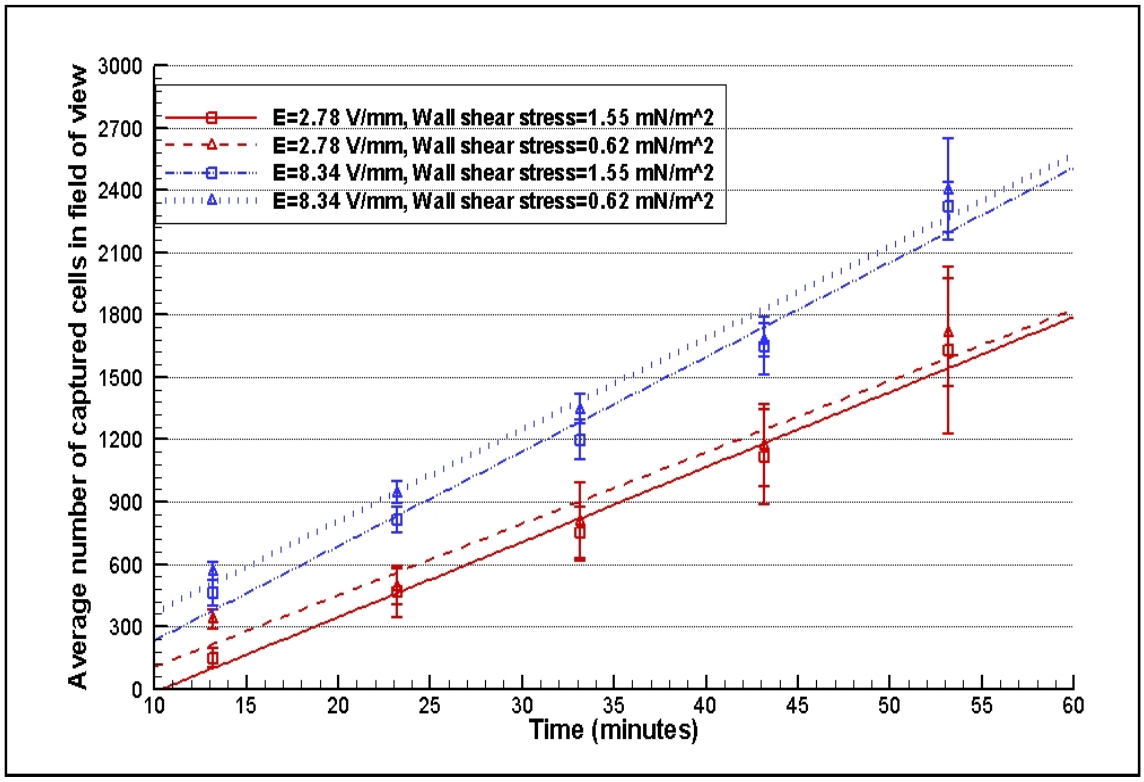

Figure 23: Time dependence of capture as a function of shear stress at two different electric fields and 6 *mL/hr* flowrate. Each data point has 380 s variation in time, induced by the experimental protocol.

At both electric fields, capture is higher at lower wall shear stress (0.62 mN/m^2) locations. However, as evidenced from the variance values, variations in the wall shear stress were not significant enough to observe drastically different capture at various locations on the electrode. In order to do this, the channel design needs to be modified to induce considerably higher variations in wall shear stress. Since the device design is

based on standard photolithographic techniques, other electrode patterns and channel designs could easily be fabricated by just using a different mask.

DISCUSSIONS

We demonstrated capture of bacterial cells suspended in phosphate buffer in a microfluidic device utilizing particle tracking with a fluorescent microscope followed by image processing. Constant cell accumulation rate was observed at both 2 and 6 *mL/hr* external flow rate with an applied potential difference of 1.0 and 1.25 *V*. Capture in the system was analyzed as a function of wall shear stress, which enabled us to identify high and low capture sites on the electrode. Sampling images at multiple locations on the electrode surface enabled us to delineate capture over the entire electrode area and identify variable capture trends at different locations on the surface.

Cell migration towards the oppositely charged electrode occurs by electrophoresis, which is dictated by the apparent electric field experienced by the particles in bulk solution. The apparent electric field at different flow rates was predicted indirectly by monitoring electric currents in the system. Detailed knowledge of the electrochemical reactions that are responsible for Faradaic currents in the buffer solution is essential to maximize electrophoresis in the system and to optimize device performance. For example, in this study, we utilized a phosphate buffer (pH=5.5, ionic strength=1 *mM*) to perform our capture experiments. The effect of buffer pH on the current is propagated through the concentration of H^+ and OH^- ions in the system. Hydrogen ions have a tendency to get reduced by accepting an electron, whereas

hydroxyl ions have a tendency to get oxidized by losing electrons. The rates of these reactions influence the Faradaic currents in the system, in a non-trivial way.

The electrochemical reactions that happen in our system are described as follows. Since we used a phosphate buffer to perform our experiments, the ions in our buffer are H^+, K^+, and PO_4^{3-} respectively. The H^+ and K^+ ions have a tendency to accept electrons from the electrode and undergo reduction reactions at the anode, which are represented as [106]

$$K^+ + e^- \rightarrow K$$

$$2H_2O + 2e^- \rightarrow H_2 + 2\ OH^- \text{ (solvent)}$$

$$2H^+ + 2e^- \rightarrow H_2 \text{ (reference electrode)}$$

Standard potentials for the above reactions are -2.92 V, -0.83 V and 0.00 V, respectively. The PO_4^{3-} ions hydrolyze in water to generate OH^- ions which then have a tendency to undergo oxidation at the cathode. These reactions are represented as

$$PO_4^{3-} + H_2O \text{ <==> } HPO_4^{2-} + OH^-$$

$$4OH^- \rightarrow 2H_2O + O_2 + 4e^-$$

Standard potential for the above reaction is -0.40 V. All the standard potentials in the reduction and oxidation reactions are the potentials at which complete reactions (as shown above) would take place. At lower potentials, these reactions may occur at smaller rates, generating Faradaic currents in the system even at lower potentials. Electric currents due to these reactions can be calculated from the rate constants, which must be determined experimentally [107].

The Faradaic processes due to the electrochemical reactions in our system can be described using the Cottrell equation [108] that explains the current transients in the system. Without flow in the system, the current can be represented as

$$I(t) = \frac{nFAD_i^{1/2}C_i}{\pi^{1/2}t^{1/2}} \tag{23}$$

where t is the time, n is the number of moles of electrons transferred in the electrochemical reaction, F is the Faradays constant, A is the electrode surface area and D_i and C_i are diffusion coefficient and concentration of ions, respectively. From equation (23), it can be seen that the main parameter that dictates the amount of Faradaic currents in the system is the number of moles of electrons transferred in the electrochemical reactions. This depends on the difference between the applied potential and the standard potentials of the ion oxidation and reduction reactions in the system. In flow based systems, this equation has to be modified to account for convection of ions. In this case, charge separation due to polarization can create concentration boundary layers along the electrode-electrolyte interface, which will vary with position. Modeling of this behavior requires detailed local information on Faradaic processes, and is not attempted in this study.

Capture results obtained in a single microchannel constitute the proof of concept for pathogen concentration in micro-scale devices. For such applications, an integrated serial microfluidic system could be used for species capture. Efficient capture of bacterial species in a single channel at large flow rates is critical to develop miniaturized systems that can sample large volumes. Capturing particles within shorter times can be

achieved by reducing the particle migration time to the anode. This would reduce the channel wetted volume by reducing the channel length, and/or increase sampling flowrate while still satisfying the $t_M<t_R$ design constraint. Smaller migration times can be achieved by decreasing the electrode spacing (h) and/or by increasing the apparent electric field in the bulk solution.

CONCLUSIONS OF IN-SITU QUANTIFICATION

We presented a microfluidic approach for continuous capture of bacterial cells suspended in phosphate buffer by applying external electric fields. The effect of flow rate, applied electric field, and wall shear stress on cell capture in the device was analyzed using particle tracking via fluorescent microscopy techniques. Analyzing capture across multiple locations on the electrode surface enabled estimation of average capture over the entire electrode area as a function of time. The device exhibits approximately linear increase in the number of average captured cells by time, which is an indication of constant cell capture rate. This was verified independently using the cell culture methods. We observed strong variations in the capture rate as a function of the externally applied electric field. However, capture rate dependence on the flowrate and capture rate at various locations with different the wall shear stress values did not result in statistically significant results. Furthermore, electrochemical reactions due to Faradaic processes play a crucial role on electrophoresis of bacterial cells towards the anode, and in adhesion of cells on to the surfaces. Presence of convective effects due to pressure driven flow further complicates analysis and optimization of cell capture in the device. Despite these caveats, capture trends presented in this study can be utilized for designing

microfluidic systems for biosensors, designed bacterial bio-films, and devices for bacterial sample concentration from large volumes.

CONCLUSIONS

We have developed a generic prototype microfluidic device to capture and concentrate various microorganisms from water. The device capture efficiency was quantified by plating and real-time PCR and the capture trends were also validated using fluorescent microscopy experiments. Based on the results presented, the device design can be modified to optimize performance, and to deliver higher concentration factors within shorter time intervals. The electrochemistry associated with DC electric fields in micro-scale devices was also presented. Further investigation of flow systems, by solving the Nernst Planck equation with convective effects is required, to better predict the time scales of current transients in the system.

The proposed device is capable of concentrating most negatively charged microbial contaminants. It can work either as a filter (capture unit) or it can be used as a sample concentration device for enhancing detection capabilities. Low power and small wetted volume of the device would enable development of portable units. Since the device design and fabrication are based on standard photolithographic techniques, it is extremely cost effective to batch fabricate multiple microchannels at one time to scale-up the device to sample large volumes. Continuous sampling of water without chemical additives enables utilization of the device upstream of potable use. Hence the device can work either as a filtration unit or as a sample concentrator that enhances capabilities of real-time detection technologies. Once completed, this device based on its design and application can be placed within distribution lines at critical junctions, at dead-end spots or at points-of-use for routine monitoring or in response to specific water quality threats.

REFERENCES

1. Olson E D 1999 Bottled Water: Pure Drink or Pure Hype? *Natural Resources Defense Council Research Report*.
2. Drysdale A E and Hanford A J 2002 Advanced life support research and development matrix *NASA-JSC* Report # 47787.
3. Ibekwe A M and Grieve C M 2003 *J. Appl. Microbiol.* **94** 421-31.
4. Vora G J, Meador C E, Stenger D A and Andreadis J D 2004 *Appl. Environ. Microbiol.* **70**(5) 3047-54.
5. Morales-Morales H A, Guadalupe V, Olszewski J, Rock C M, Dasgupta D, Oshima K H and Smith G B 2003 *Appl. Environ. Microbiol.* **69**(7) 4098-102.
6. Koros W J, Ma Y H and Shimadzu T 1996 *Pure Appl. Chem.* **68** 1479-89.
7. G.E. Water and Process Technologies http://www.gewater.com/products/equipment/mf_uf_mbr/mf.jsp (accessed April 18, 2006).
8. Singh R P and Heldman D R 1993 *Introduction to Food Engineering, 2nd edn*. (San Diego: Academic Press Inc).
9. Nield A D and Bejan A 1999 *Convection in Porous Media* (New York: Springer Verlag).
10. G.E. Osmonics http://www.osmonics.com/library/mfh.htm (accessed May 1, 2006).

11. Hou K, Gerba C P, Goyal S M and Zerda K S 1980 *Appl. Environ. Microbiol.* **40** 892-6.

12. Argonide http://www.argonide.com/nanoceram_filters2.pdf (accessed June 1, 2006).

13. Hill V R, Polaczyk A L, Donghyun H, Narayanan J, Cromeans T L, Roberts J M and Amburgey J E 2005 *Appl. Environ. Microbiol.* **71**(11) 6878-84.

14. Goyal S M and Gerba C P 1980 *Appl. Environ. Microbiol*. **40**(5) 912–6.

15. Winona L J, Ommani A W, Olszewski J, Nuzzo J B and Oshima K H 2001 *Can. J. Microbiol.* **47** 1033-41.

16. Busalmen J P and de Sánchez S R 2001 *Appl. Environ. Microbiol.* **67**(7) 3188-94.

17. Lapizco-Encinas B H, Simmons B A, Cummings E B and Fintschenko Y 2004 *Electrophoresis* **25**(10-11) 1695 –704.

18. Halle K J, Li J J, Munson M S, Monteith J, Guzman E, Feather S, Verba J, Porter Q, Kenning V, Kamholz A E, Weigl B H, Saltsman P, Bardell R and Yager P 2003 *Proc.International Conference on Miniaturized Chemical and Biochemical Analysis Systems* (Squaw Valley, CA) pp. 559-63.

19. Cabrera C R and Yager P 2001 *Electrophoresis* **22** 355-62.

20. Lapizco Encinas B H, Simmons B A, Cummings E B and Fintschenko Y 2004 *Anal. Chem*. **76**(6) 1571-79.

21. Weimer C, Walsh M K, Beer C, Koka R and Wang X 2001 *Appl. Environ. Microbiol.* **67** 1300-07.

22. Boyle M, Ford T, Maki J S and Mitchell R 1991 *Waste Manag Res.* **9** 465-70.

23. Noda Y and Kanemasa Y 1984 *Physiol Chem Phys Med NMR* **16**(4) 263-74.

24. Schijven J F 2001 Ph.D. Dissertation Delft: Technical University.

25. Wilson W W, Wade M M, Holman S C and Champlin F R 2001 *J. Microbiol. Methods* **43** 153-64.

26. Peterson A A, Hancock R E W and McGroarty E J 1985 *J. Bacteriology* **164** 1256-61.

27. Jucker B A, Harms H and Zehnder A J 1996 *J. Bacteriol.* **178** 5472-79.

28. Bayer M E and Sloyer J L 1990 *J. Gen. Microbiol* **136** 867-74.

29. Buggs C W and Green R C 1935 *J. Bacteriol.* **30** 447-51.

30. Collins Y E and Stotzky G 1992 *Appl. Environ. Microbiol*. **58** 1592-600.

31. Collins Y E and Stotzky G 1996 *Can. J. Microbiol*. **42** 621-27.

32. Glynn J R Jr, Belongia B M, Arnold R G, Ogden K L and Baygents J C 1998 *Appl. Environ. Microbiol.* **64**(7) 2572-77.

33. Nomura S, Kuroiwa A and Nagayama A 1995 *Chemotherapy.* **41** 77-81

34. Zewen L, Chen W and Papadopoulos K D 1999 *Environ Microbiol.* **1**(1) 99-102.

35. Derjaguin B V and Landau L D 1941 *Acta Physicochim. URSS* **14** 733-62.

36. Verwey E J W and Overbeek J Th 1948 *Theory of the Stability of Lyophobic Colloids* (New York: Elsevier).

37. Hermansson M 1999 *Biointerfaces* **14** 105-19

38. Poortinga A T, Bos R, Norde W and Busscher H J 2002 *Surface Science Reports* **47** 1-32.

39. Karniadakis G, Beskok A and Aluru N 2005 *Miroflows and Nanoflows: Fundamentals and Simulation* (New York: Springer).

40. Mark C M, Loosdrecht V, Johannes L, Norde W and Zehnder A J B 1990 *Microbiological Reviews* **54**(1) 75-87.

41. Hubbard A T 2002 *Encyclopedia of Surface and Colloid Science: Volume 3* (New York: Dekker).

42. Codony F, Morato J and Mas J 2005 *Water Res.* **39** 1896-1906.

43. Endley S, Lu L, Vega E, Hume M E and Pillai S D 2003 *J Food Prot.* **66**(1), 88-93.

44. Lee J S, Ray R I, Lemieux E J, Falster A U and Little B J 2004 *Biofouling* **20** 237-47.

45. Song B and Leff L G 2005 *Microbiol Res.* **160** 111-17.

46. Stine S W, Song I, Choi C Y and Gerba C P 2005 *J Food Prot.* **68**(5) 913-8.

47. Gagnon G A, Rand J L, O'Leary K C, Rygel A C, Chauret A C and Andrews R C 2005 *Water Res.* **39**(9) 1809-17.

48. Lehtola M J, Miettinen I T, Lampola T, Hirvonen A, Vartiainen T and Martikainen P J 2005 *Water Res.* **39**(10) 1962-71.

49. USEPA 2000 *Improved Enumeration Methods for the Recreational Water Quality Indicators: Enterococci and Escherichia coli* EPA. 821/R-97/004.

50. Dowd S E, Pillai S D, Wang S and Corapcioglu M Y 1998 *Appl. Environ. Microbiol.* **64** 405-10.

51. Grant S B, List E J and Lidstrom M E 1993 *Water Res.* **29** 2067-85.

52. Guan H, Schulze-Makuch D, Schaffer S, Pillai S D 2003 *Groundwater.* **41** 701-8.

53. Hassan A N and Frank J F 2004 *Int J Food Microbiol.* **96**(1) 103-9.

54. Pereira da Silva C H, Vidigal Jr G M, De Uzeda M and De Almeida Soares G 2005 *Implant Dent.* **14**(1) 88-93.

55. Boyle M, Ford T, Maki J S and Mitchell R 1991 *Waste Manag Res.* **9** 465-70.

56. Noda Y and Kanemasa Y 1984 *Physiol Chem Phys Med NMR*. **16**(4) 263-74.

57. Schijven J F 2001 Ph.D. Dissertation (Delft: Technical University).

58. Wilson W W, Wade M M, Holman S C and Champlin F R 2001 *J. Microbiol. Methods* **43** 153-64.

59. Bayer M E and Sloyer J L 1990 *J. Gen. Microbiol* **136** 867-74.

60. Buggs C W and Green R C 1935 *J. Bacteriol.* **30** 447-51.

61. Collins Y E and Stotzky G 1992 *Appl. Environ. Microbiol*. **58** 1592-600.

62. Collins Y E and Stotzky G 1996 *Can. J. Microbiol*. **42** 621-27.

63. Glynn J R Jr, Belongia B M, Arnold R G, Ogden K L and Baygents J C 1998 *Appl. Environ. Microbiol.* **64**(7) 2572-77.

64. Nomura S, Kuroiwa A and Nagayama A 1995 *Chemotherapy.* **41** 77-81

65. Zewen L, Chen W and Papadopoulos K D 1999 *Environ Microbiol.* **1**(1) 99-102.

66. Lytle D A, Rice E W, Clifford H and Fox K R 1999 *Appl. Environ. Microbiol.* 3222-5.

67. Dongsheng D, Chen Y, Qi L and Yu X 2003 *Electrophoresis* **24** 3219–23.

68. Henny C V and Busscher H J 2001 *Appl. Environ. Microbiol.* **67**(2) 491-4.

69. Beckman Coulter http://www.beckmancoulter.com/Literature/BioResearch/DS-8284A.pdf (accessed January 2005).

70. Kourkine I V, Mirjana R P, Davis E, Ruffolo C G, Kapasalis A and Annelise Barron A E 2003 *Electrophoresis* **24** 655-61.

71. Buszewski B, Szumski M, Klodzinska E and Dahm H 2003 *J. Sep. Sci.* **26** 1045-49.

72. Wilson K and Walker J 2005 *Principles and Techniques of Biochemistry and Molecular Biology*, 6th Edition (New York: Cambridge University Press).

73. Lee J S, Ray R I, Lemieux E J, Falster A U and Little B J 2004 *Biofouling* **20** 237-47.

74. Abramoff M D, Magelhaes P J, Ram S J 2004 *ImageJ. Biophotonics International* **11**(7) 36-42.

75. Lyman R, Longnecker M 2001 *An Introduction to Statistical Methods and Data Analysis*, 5th edition (New York: John Wiley).

76. Kilian H G, Gruler H, Bartkowiak D and Kaufmann D 2005 *Eur. Phys. J. E* **17** 307-25.

77. Givskov M, Eberl L, Poulsen S M, Molin L M S 1994 *J. Bacteriol.* **176**(1) 7-14.

78. Lewis P J, Nwoguh C E, Barer M R and Harwood C R 1994 *Mol. Microbiol.* **13**(4) 655-62.

79. Marco-Noales E, Biosca E G and Amaro C 1999 *Appl. Environ. Microbiol.* **65**(3) 1117-26

80. Roszak D B, Colwell R R 1987 *Microbiol Rev.* **51**(3) 365-79.

81. Jones J F, Feick J D, Imoudu D, Chukwumah N, Vigeant M and Velegol, D 2003 *Appl. Environ. Microbiol.* **69**(11) 6515-9.

82. Hayashi H, Tsuneda S, Hirata A, Sasaki H 2001 *Biointerfaces* **22** 149–57

83. Lytle D A, Rice E W, Clifford H and Fox K R 1999 *Appl. Environ. Microbiol.* **65**(7) 3222-5.

84. Campos J L, Garrido J M, Mendez R and Lema J M 2001 *Appl. Biochem. Biotechnol*. **95**(1) 1-10.

85. Daly B, Betts W B, Brown A P and O'Neill J G 1998 *Microbios* **96**(383) 7-21.

86. Hunt S M, Werner E M, Huang B, Hamilton M A and Stewart P S 2004 *Environ. Microbiol*. **70**(12) 7418-25.

87. Bard A J and Faulkner L R 2001 *Electrochemical Methods: Fundamentals and Application* (New York: John Wiley).

88. Fox R W, McDonald A T and Pritchard P J 2005 *Introduction to Fluid Mechanics,* 6th Edition *(*New York: John Wiley & Sons).

89. Vega E, Smith J, Garland J, Matos A and Pillai S D 2005 *J. Food Prot.* **68**(10) 2112-7.

90. Borchardt M and Lambertini E 2005 *(UC-Davis and Marshfield Clinic Research Foundation)* Research report.

91. Gad-el-Hak M 2005 *MEMS Handbook,* 2nd Edition (Boca Raton, FL: CRC Press).

92. Bruening 2003 *Langmuir* **19** 7038-42.

93. Yang J, Bos R, Poortinga A T, Wit P J, Belder G F and Busscher H J 1999 *Langmuir* **15** 4671-7.

94. Poortinga A T, Bos R and Busscher H J 1999 *Journal of Microbiological Methods* **38** 183–9.

95. Poortinga A T, Bos R and Busscher H J 2000 *Biotechnology and Bioengineering* **67**(1) 117-20.

96. Meinders J M, Noordmans J and Busscher H J 1992 *Journal of Colloid and Interface Science* **152**(1) 265-80.

97. Sjollema J and Busscher H J 1999 *Colloids and Surfaces* **41** 323-36.

98. Abbott A, Berkeley R C W and Rutter P R 1980 Sucrose and the deposition of Streptococcus mutans at solid liquid interfaces *Microbial Adhesion to Surfaces* ed Berkeley R C W, Lynch J M, Melling J, Rutter P R and Vincent B (Chichester: Ellis Horwood:) pp 117-42.

99. Maruyama A and Sunamura M 2000 *Appl Environ Microbiol* **66**(5) 2211–5.

100. Bazant M Z, Thornton K and Ajdari A 2004 *Phys. Rev. E* **70** 021506.

101. Hahm J, Balasubramanian A K and Beskok A 2007 *Physics of Fluids* **19** 013601.

102. Gustafsson B and Vasilev A 2006 *Conformal and Potential Analysis in Hele-Shaw Cells, Advances in Mathematic Fluid Mechanics* (Berlin, Germany: Springer) pp 20-68.

103. Fluent http://www.fluent.com/software/gambit/index.htm (Accessed October 2006).

104. RSB Schalungskchnik http://rsb.info.nih.gov/ij/ (Accessed September 2006).

105. Hermansson M 1999 *Colloids and Surfaces B: Biointerfaces* **14**(1) 105-19.

106. Bard A J, Parsons R and Jordan J 1985 *Standard Potentials in Aqueous Solution* (New York: CRC Press).

107. Bard A J and Faulkner L R 2001 *Electrochemical Methods: Fundamentals and Applications* (New York: John Wiley).

108. Brett C M A and Brett A M O 1993 *Electrochemistry: Principles, Methods, and Applications* (Cary, NC: Oxford University Press) pp 200-210.

VITA

Name: Ashwin Kumar Balasubramanian

Address: 800, Marion Pugh, Apt 301

College Station, TX 77840

Email Address: bashwin@neo.tamu.edu

Education: B.Tech, Indian Institute of Technology, Madras, India, 2000

M.S., Texas A&M University, College Station, Texas, 2003

Ph.D., Texas A&M University, College Station, Texas 2007